

Dissertation
submitted to the
Faculty for Mathematics and Computer Science
of the Ruperto-Carola University of Heidelberg, Germany
for the degree of
Doctor of Natural Sciences

presented by

Dipl. Math. Melanie Rinas

born in Bad Saulgau, Germany

Oral-examination: _____

Modeling the antiviral interferon response against viral infections on varied terrain

Referees: Prof. Dr. Anna Marciniak-Czochra
Prof. Dr. Thomas Höfer

Declaration

The applicant, Melanie Rinas, declares that she is the sole author of the submitted dissertation and no other sources or materials from those specifically referred to have been used.

In addition, the applicant declares that she has not applied for permission to enter examination procedure at another institution and this dissertation has not been presented to ~~other~~ faculty and not used in its current or in any other form in another examination.

Date

Signature

Contents

Abstract	i
Zusammenfassung	iii
1 Introduction	1
1.1 Research on the antiviral interferon defense	1
1.2 Outline of this thesis	1
2 Stochastic modeling predicts paracrine propagation of the IFN response	3
2.1 Experimental study of the IFN system revealed multi-layered stochasticity in individual cells	4
2.1.1 Monitoring virus-induced IFN induction and response at single-cell level	4
2.1.2 Cell-to-cell variability in IFN induction	5
2.1.3 IFN target gene induction is an all-or-nothing switch	11
2.2 Stochastic model of the IFN response against viral infection	14
2.3 Model simulations based on Gillespie's algorithm	18
2.4 Estimation of model parameters	22
2.4.1 Parameter determination for the virus-induced activation of the transcription factors of IFN	22
2.4.2 Parameter determination of the IFN expression	25
2.4.3 Parameter determination of the IFN response	28
2.5 Stochastic modeling exposes individual IFN producers as sentinels of viral infection	30
3 Spatio-temporal stochastic model of IFN response against viral spread demonstrates homogeneous diffusion	33
3.1 Dissecting the dynamics of IFN-induced antiviral defense against spreading DENV in living cells	33
3.1.1 Detection of DENV infection and antiviral IFN response at single-cell level	33
3.1.2 The competition between spreading DENV and IFN-induced antiviral protection	34
3.2 Reaction-diffusion model of viral spread and cell communication through secreted IFN	34
3.3 Spatio-temporal model simulations show no strong gradients of extracellular virus and IFN	34

4 Population-based modeling reveals major control of viral fitness by the antiviral effect of IFN on already infected cells	35
4.1 Quantification of viral spread and the antiviral IFN response	35
4.1.1 Observation of antiviral protection against DENV-wt infection through IFN stimulation	35
4.1.2 Examination of viral fitness by comparing DENV-wt with a DENV mutant lacking 2'-O-methylation activity	35
4.2 Population-based delay-differential equation model of viral spread and IFN-induced antiviral defense	35
4.3 Parameterization of the DDE model	35
4.3.1 Estimation of model parameters by using DENV-wt measurements	35
4.3.2 Detection of DENV mutant specific model parameters by utilizing the knowledge from wt-fitting	35
4.4 Population-based model predicts strong limitation of viral spread through the impact of IFN on virus production rate	35
5 Discussion	37
Publications and presentations	39
Bibliography	40
Abbreviations and symbols	46
Acknowledgments	51

Abstract

Zusammenfassung

1 Introduction

1.1 Research on the antiviral interferon defense

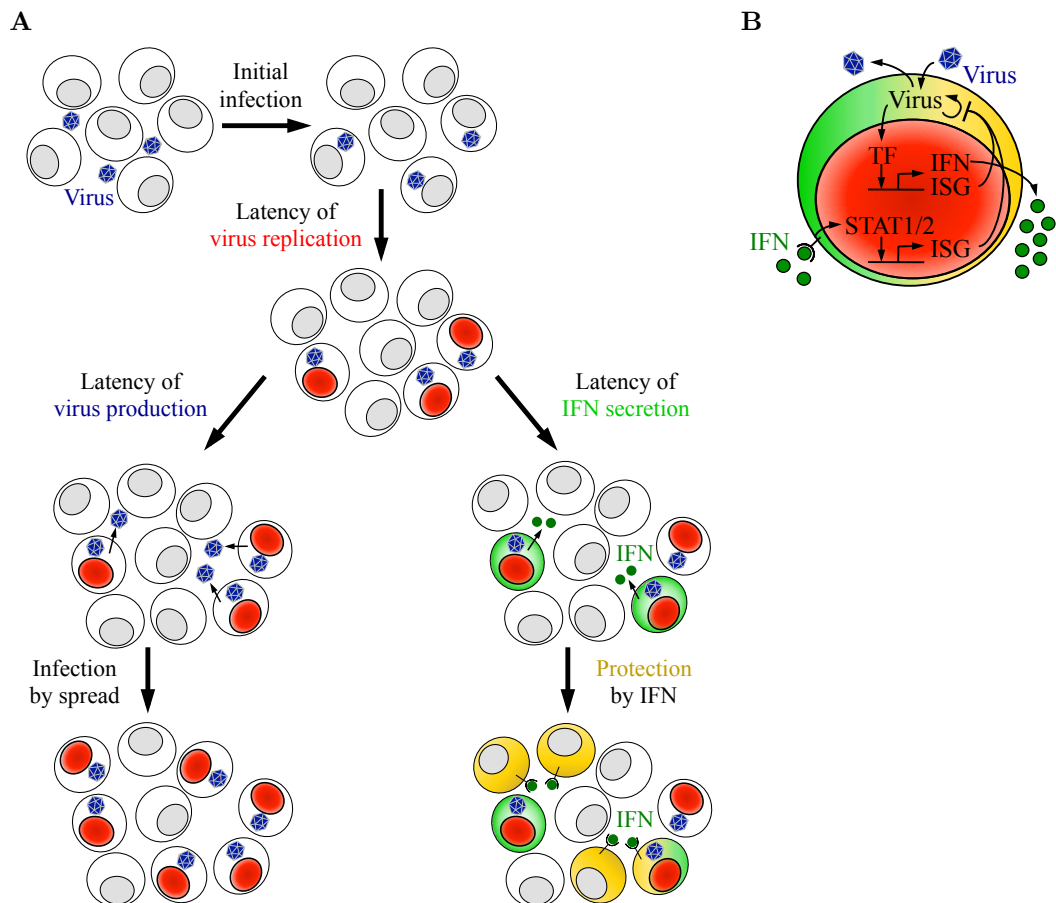


Figure 1.1: (A) Population level (B) Single cell level

1.2 Outline of this thesis

2 Stochastic modeling predicts paracrine propagation of the IFN response

The interferon (IFN) system, as the first line of defense against viral infections, has a central antiviral function (Kunzi and Pitha (2003), Sadler and Williams (2008), Takeuchi and Akira (2009)). Since the expression of IFN is crucial to induce an antiviral protective state, it is quite surprising that only a fraction of cells in a virus-infected cell population induces IFN (Zawatzky et al. (1985), Hu et al. (2007)).

 The literature contains various reasons for the observed cell-to-cell variability in IFN expression. Some studies have suggested that host cell-intrinsic causes, such as a mechanism of IFN gene induction (Hu et al. (2007), Apostolou and Thanos (2008)) or cellular variance in expression of the viral sensor protein retinoic-acid inducible gene-I (RIG-I) (Hu et al. (2011)) lead to heterogeneous IFN production. Alternatively, the infecting virus was attributed to be responsible for the stochasticity in IFN induction (Chen et al. (2010), Killip et al. (2011)). According to the involved cell type or virus it could be that multiple factors contribute to the heterogeneity in IFN induction.

To study cell-to-cell variability of the IFN system our cooperation partners Dr. Ulfert Rand, Dr. Mario Köster and Dr. Hansjörg Hauser from the Department of Gene Regulation and Differentiation at the Helmholtz Centre for Infection Research (HZI) in Braunschweig established a set of reporter constructs to monitor successive steps of IFN induction and response in single cells (cf. section 2.1.1, Rand and Hauser (2010)). Live-cell imaging data demonstrate that all key steps of the IFN system - the virus-induced signal transduction, the IFN expression (cf. section 2.1.2), and the induction of IFN-stimulated genes (ISGs) (cf. section 2.1.3) - are stochastic events in single cells. Additional experiments revealed that cell-intrinsic variability contributes to the detected heterogeneity in IFN induction (cf. section 2.1.2). Besides we examined the response to IFN and discovered a dose-dependent binary pattern of two distinct subpopulations (cf. section 2.1.3). The IFN responding subpopulation achieves an antiviral protection whereas virus can still replicate in the non-responding cell fraction.

Based on the observed stochastic dynamics of the IFN network we established a multi-scale mathematical model using Gillespie's algorithm (cf. sections 2.2 - 2.4). The model describes the intracellular viral replication and the expression of IFN and ISGs in individual cells together with the intercellular communication through secreted IFN. Our simulations, which could be verified experimentally, predict that a small fraction of IFN-producing cells are sufficient to induce IFN target genes in

2 Stochastic modeling predicts paracrine propagation of the IFN response

the other, non-producing cells of the population (cf. section 2.5). Thus, we assume, that the stochastic sensing of viral infections by the innate immune system together with the paracrine signal propagation provide an efficient and viral-load sensitive mechanism to limit viral spread (Rand, Rivas et al. (2012)).

2.1 Experimental study of the IFN system revealed multi-layered stochasticity in individual cells

2.1.1 Monitoring virus-induced IFN induction and response at single-cell level

The finding that only a fraction of infected cells induces IFN (Zawatzky et al. (1985), Hu et al. (2007)) demonstrates the need to investigate the IFN system at single-cell level. A valuable method to monitor the dynamics and variability of individual cells in real time is live imaging (Spiller et al. (2010)). The first live-cell analysis for the IFN system was realized by our collaboration partners Dr. Ulfert Rand, Dr. Mario Köster and Dr. Hansjörg Hauser from the Department of Gene Regulation and Differentiation at the Helmholtz Centre for Infection Research (HZI) in Braunschweig (Rand and Hauser (2010)).

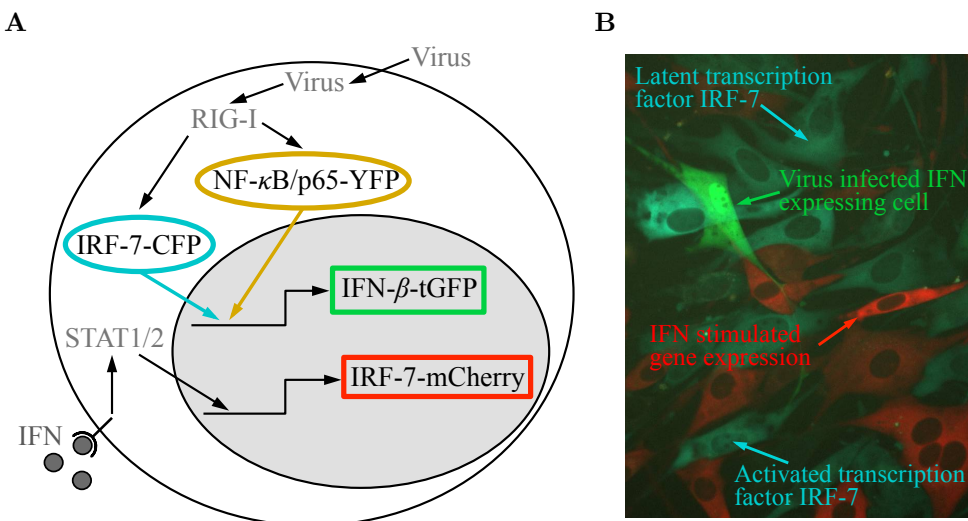


Figure 2.1: Key steps of the IFN pathway can be monitored with constructed fluorescence reporter cells. (A) Scheme of the established intracellular reporters. Virus recognition by RIG-I causes the nuclear translocation of the fusion proteins IRF-7-CFP (cyan nucleus) and NF-κB/p65-YFP (yellow nucleus). Subsequent IFN- β expression becomes visible through the BAC reporter IFN- β -tGFP (green cytoplasm) and induces the expression of ISGs illustrated by the BAC construct IRF-7-mCherry (red cytoplasm). (B) Fluorescence picture of the established intracellular reporters. The virus-induced activation of the latent transcription factor IRF-7 (cyan cytoplasm) lead to its nuclear translocation (cyan nucleus). The following expression of IFN (green cytoplasm) results in the induction of ISGs (red cytoplasm). (Experiments by U. Rand, M. Köster and H. Hauser)

2.1 Experimental study of the IFN system revealed multi-layered stochasticity

Hauser and colleagues developed fluorescence reporter cells to visualize successive key steps of the IFN system consisting of (i) virus-induced signal transduction, (ii) IFN expression and (iii) IFN response (Figure 2.1). The signal transduction after the recognition of virus by the intracellular receptor RIG-I results in the nuclear translocation of the nuclear factor κ B (NF- κ B) as well as the IFN regulatory factor (IRF) 7 (Brennan and Bowie (2010)). To observe the nuclear translocation of these transcription factors (TFs), the scientists at the HZI designed dual reporter cells which were labeled with the fluorescent markers NF- κ B/p65-YFP and IRF-7-CFP, respectively. The presence of transcription factors in the nucleus induces IFN including IFN- β (leofilopoulos et al. (2005)), which was monitored by transfecting murine fibroblasts with a bacterial artificial chromosome (BAC) encoded reporter expressing TurboGFP under the control of the IFN- β promoter (IFN- β -tGFP). Another BAC-based reporter construct in which the mCherry gene is linked to the C-terminal end of the genomic IRF-7 sequence (IRF-7-mCherry) enables the investigation of the prototypical ISG IRF-7 in response to secreted IFN (Honda et al. (2005)). All reporter constructs were transfected into murine NIH3T3 fibroblasts and representative stable cell clones (Rand, Rinas et al. (2012); Supplementary Figure S2 and Supplementary Figure S8, Rand and Hauser (2010)) were utilized for the studies.

2.1.2 Cell-to-cell variability in IFN induction

In order to examine the properties of virus-induced IFN expression, we used for infection the enveloped single-stranded RNA Newcastle Disease Virus (NDV). The paramyxovirus NDV causes the contagious Newcastle disease in birds and a close contact to infected animals can trigger conjunctivitis as well as influenza-like symptoms in humans (Capua and Alexander (2004)). After infection NDV replicates and induces IFN cells via the viral RNA sensor RIG-I (Kato et al. (2005), Childs et al. (2007)), but cannot generate new infectious virus particles (Rott (1979)). Therefore our experimental setup allows the examination of IFN induction after primary infection.

As we are primarily interested in single-cell behavior of IFN expression, we firstly monitored by time-lapse microscopy IFN- β -tGFP reporter cells (cf. section 2.1.1) after infection with different doses of NDV given in haemagglutinating unit per milliliter (HAU/ml) (Figure 2.2A left and Rand, Rinas et al. (2012); Supplementary Movie S1). The IFN- β -producing cells started at various times to express IFN- β with cell-to-cell differences as large as 10 h. Although we detected earlier onset of IFN- β -tGFP induction after infection with higher viral loads, the relative variability or “noise” (Swain et al. (2002), Elowitz et al. (2002), Kærn et al. (2005)) which can be calculated with the 5 \log_{10} coefficient of variation (CV; standard deviation divided by mean) varied only slightly (Figure 2.2A top right).

Besides we analyzed if the temporal heterogeneity in IFN- β expression is determined by varying times of infection or due to intrinsic features of the host cell. Therefore we bypassed viral infection through liposome transfection of the viral-surrogate poly I:C (polyinosinic-polycytidyllic acid) stimuli (liposome-free delivery of poly I:C did

2 Stochastic modeling predicts paracrine propagation of the IFN response

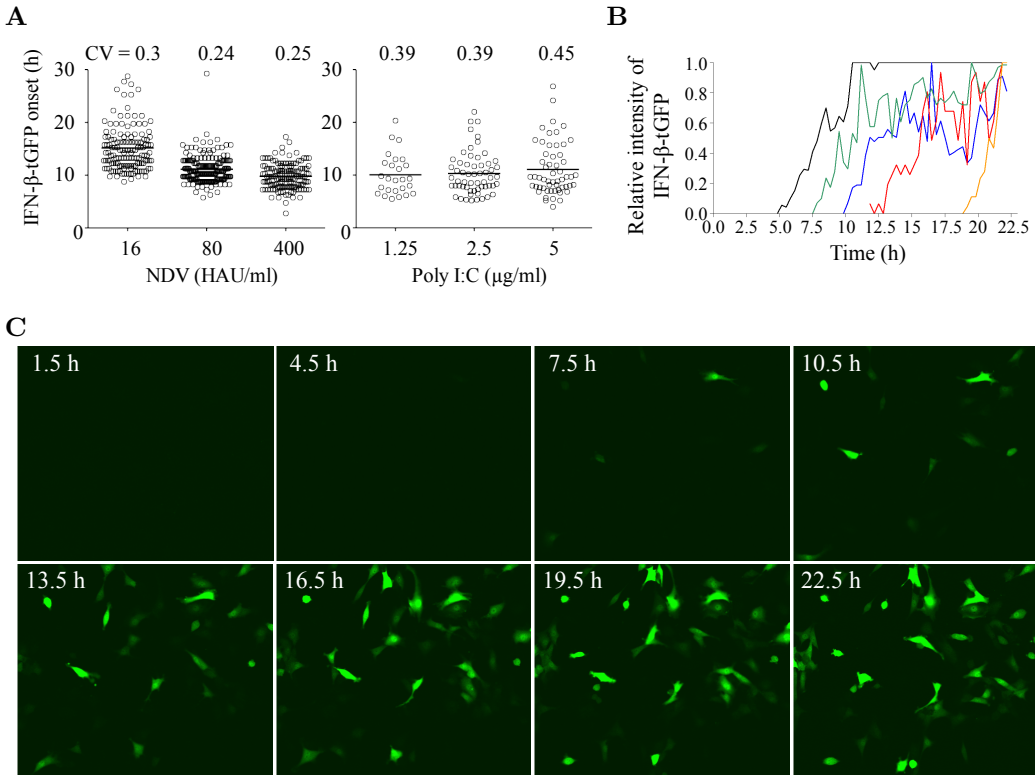


Figure 2.2: Cell-to-cell heterogeneity in onset of IFN- β expression. (A) Single-cell variability in IFN- β induction is virus-independent. IFN- β -tGFP reporter cells were infected for 1 h with different doses of NDV (x-axis, left) or transfected with varying concentrations of poly I:C (x-axis, right). Onset of IFN- β -tGFP expression (y-axis) was detected by time-lapse microscopy at 15 min intervals. The scatter plots show the distribution of 456 NDV infected cells or 140 poly I:C transfected cells, respectively. Experiment-related coefficient of variation (CV) is given at the top. (B, C) Live imaging illustrates heterogeneous IFN- β induction in individual cells. Stimulation of IFN- β -tGFP cells with 32 μ g/ml poly I:C and subsequent monitoring via time-lapse microscopy every 20 min. Selected single-cell kinetics in (B) and fluorescence pictures at indicated time post stimulation in (C) are presented. (Experiments by U. Rand, M. Köster and H. Hauser)

not induce IFN- β expression into IFN- β -tGFP reporter cells (Figure 2.2A right, B and C). Also after transfection with different poly I:C concentrations we observed an extremely heterogeneous onset of IFN- β expression in individual cells, which was quantitatively comparable to viral infection according to the same order of magnitude of the CVs (Figure 2.2A top right). These data reveal that the cell-to-cell variance in IFN- β expression is predominantly of cellular origin.

To quantitatively determine viral replication and IFN induction in single cells, IFN- β -tGFP reporter cells were infected with NDV and subjected to flow cytometry. At several time points post-infection (p.i.) we measured simultaneously the viral protein, hemagglutinin-neuraminidase (HN), and the IFN- β -tGFP intensity (Figure 2.3A and B). The fraction of virus replicating cells showed an increase over time, followed by an about 12 h delayed rising number of IFN- β -tGFP-positive cells. As in other findings (Kumagai et al. (2009), Rehwinkel et al. (2010)), we detected IFN- β -tGFP expression only in cells with replicating virus. However, a remarkable number of

2.1 Experimental study of the IFN system revealed multi-layered stochasticity

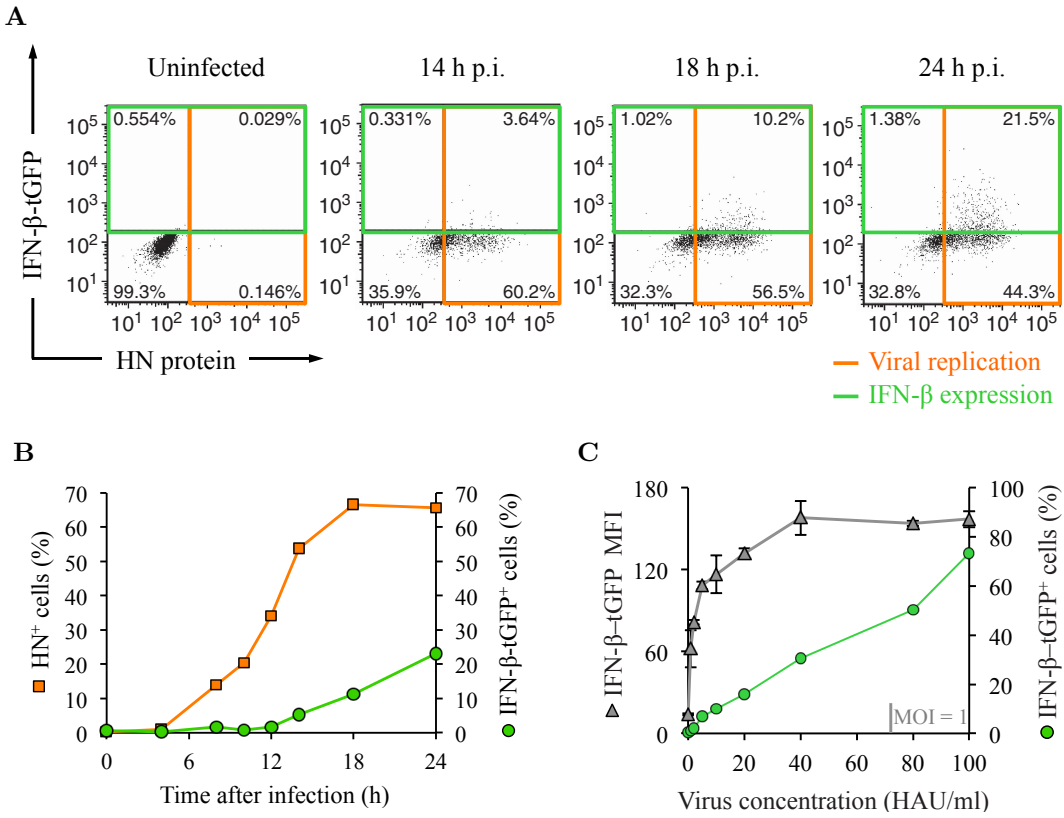


Figure 2.3: Quantitative and temporal heterogeneity in IFN- β expression. (A, B) Viral replication is necessary but not sufficient to activate IFN- β expression. IFN- β -tGFP reporter cells infected with 40 HAU/ml NDV for 1 h were subjected to flow cytometry at indicated time points post-infection. Representative dot plots in (A) illustrate the jointly measured viral HN protein (x-axis) as well as IFN- β -tGFP (y-axis) of individual cells, while the corresponding kinetics of virus-replicating cells (HN^+ , orange color) and IFN- β expressing cells ($\text{IFN-}\beta\text{-tGFP}^+$, green color) are shown in (B). (C) Secreted IFN is determined by the fraction of IFN-producing cells. IFN- β -tGFP reporter cells were infected with 1, 2, 5, 10, 20, 40, 80 or 100 HAU/ml NDV and analyzed by flow cytometry 24 h after infection. With viral load increasing fraction of IFN- β positive cells ($\text{IFN-}\beta\text{-tGFP}^+$, green color) and geometric mean of their fluorescence intensity (MFI, gray color, mean of triplicate measurements and error bars) are illustrated. (Experiments by U. Rand, M. Köster and H. Hauser)

infected cells did not express IFN. To analyze this phenomenon further, we divided the amount of infected cells into two groups according to high and low extent of viral replication (Rand, Rinas et al. (2012): Supplementary Figure S3). Since both subpopulations contained nearly the same fraction of IFN- β -tGFP-positive cells, we found no correlation between viral replication level and frequency of IFN- β -tGFP expressing cells. In the literature it was discussed, that maybe the absence of IFN-inducing viral RNA is responsible for the heterogeneity in IFN expression (Killip et al. (2011)). Thus we transfected intracellular RNA of IFN-producing and non-producing cells into naïve IFN- β -tGFP reporter cells (Rand, Rinas et al. (2012): Figure 2C and Supplementary Figure S4). As both RNA transfections activated a comparable fraction of IFN- β -tGFP-positive cells, heterogeneous IFN induction appears although IFN-inducing viral RNA is present. These results demonstrate

2 Stochastic modeling predicts paracrine propagation of the IFN response

that viral replication is necessary to induce IFN but not sufficient.

Moreover, we investigated the properties of IFN- β -tGFP expression after infection with different virus doses (Figure 2.3C). The fraction of IFN- β -tGFP-positive cells increased almost linearly with higher virus concentrations and a multiplicity of infection (MOI; number of infectious virus particles divided by number of host cells) of 1 induced IFN expression in less than half of the IFN- β -tGFP reporter cells. In contrast, the mean fluorescence intensity (MFI) of IFN- β expression reached $\sim 70\%$ of its maximum already at very low virus titer. Therefore, virus-induced IFN- β production is dominated by the fraction of IFN expressing cells.

To examine mechanistically how cell-to-cell variability in IFN expression arises, we had a closer look on the IFN induction pathway. We analyzed the virus-induced activation of the key transcription factors NF- κ B and IRF-7 by utilizing the dual reporter cells expressing NF- κ B/p65-YFP and IRF-7-CFP (cf. section 2.1.1). After infection with NDV, initially latent transcription factors NF- κ B and IRF-7 were located in the cytoplasm and subsequently translocated into the nucleus due to activation by viral sensing (Figure 2.4A). The nuclear translocation of both transcription factors happened simultaneously in a single cell, but this joint translocation time varied strongly between different cells from 7 to 20 h post infection (Figure 2.4B). We also observed a joint translocation time of the transcription factors NF- κ B/p65 and IRF-3 in individual cells by antibody staining of endogenous NF- κ B/p65 as well as IRF-3 after infection with NDV or transfection with poly I:C (Rand, Rinas et al. (2012): Supplementary Figure S6). The discovery of a single cell specific but in the cell population diverse translocation time of transcription factors demonstrates that strong cell-to-cell heterogeneity in IFN induction originates already in the shared upstream activation pathway of NF- κ B and IRF-7.

Additionally, we studied the relation between transcription factor activation and IFN induction using dual reporter cells expressing IRF-7-CFP together with IFN- β -tGFP (Figure 2.4C and Rand, Rinas et al. (2012): Supplementary Figure S7). Most of the cells (91% at 80 HAU/ml NDV) with activated transcription factor IRF-7 also expressed IFN afterwards (Figure 2.4D). The few cells (9% at 80 HAU/ml NDV) which exhibited no IFN- β expression showed similar distributed IRF-7 nuclear translocation times as the IFN- β producing cells (Figure 2.4D bottom part). Since we found no IFN- β -tGFP induction without prior nuclear translocation of IRF-7, activation of IRF-7 is absolutely necessary for IFN- β production. Thus we suggest that the decision to express IFN is primarily taken upstream of transcription factor activation.

Furthermore, the signaling delay from viral infection to IRF-7 nuclear translocation (T_{sig} ; $\bar{T}_{\text{sig}} = 11.7 \pm 4.0$ h) was almost as different among individual cells as already detected with the dual reporter cells expressing the fusion proteins NF- κ B/p65-YFP and IRF-7-CFP (Figure 2.4B; $\bar{T}_{\text{sig}} = 11.9 \pm 3.4$ h). But also the period of time between nuclear translocation of IRF-7 and onset of IFN- β -tGFP expression (T_{gen} ; $\bar{T}_{\text{gen}} = 3.4 \pm 1.5$ h) differed remarkably from cell-to-cell. The similar CVs of T_{sig} ($\text{CV}_{\text{sig}} = 0.34$) and T_{gen} ($\text{CV}_{\text{gen}} = 0.44$) indicate a comparable variability of virus-induced signal transduction and subsequent IFN- β -tGFP gene expression. Therefore, these quantitative data reveal that both transcription factor activation

2.1 Experimental study of the IFN system revealed multi-layered stochasticity

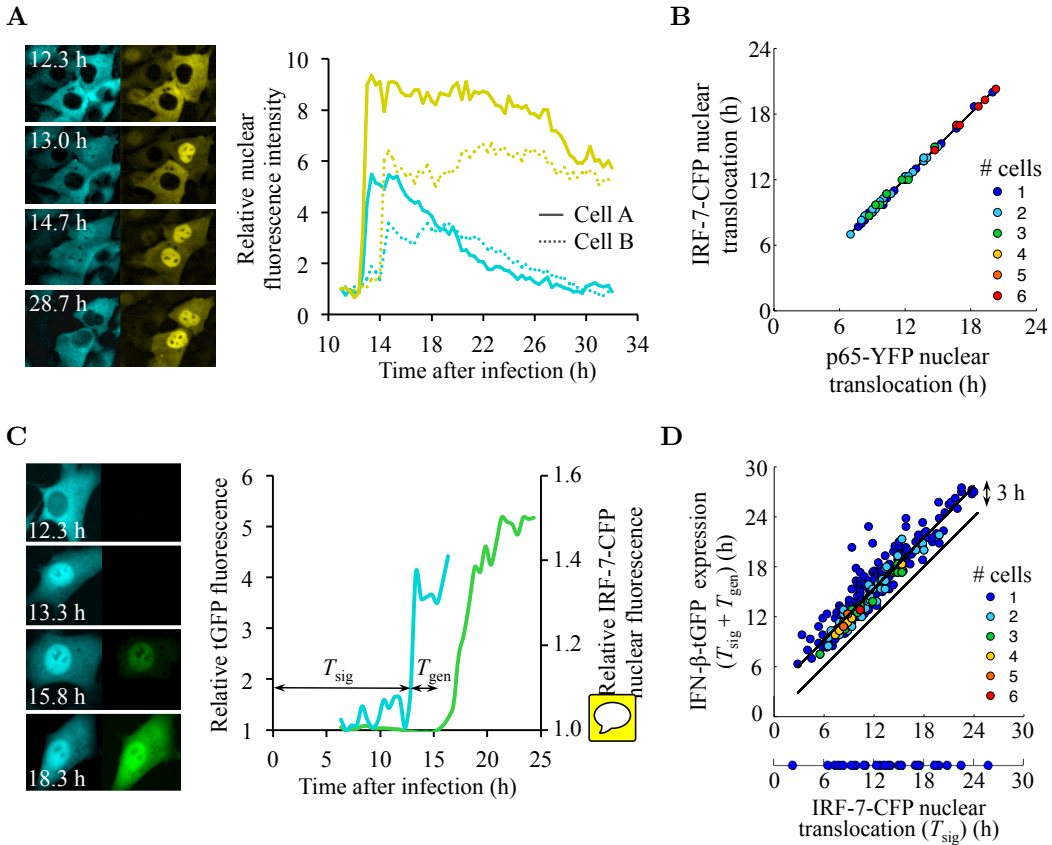


Figure 2.4: Both virus-induced signal transduction and IFN expression are sources of heterogeneity. (A, B) Synchronous translocation time of transcription factors in single cells varies at the cell population level. Dual reporter cells expressing the fusion proteins NF- κ B/p65-YFP and IRF-7-CFP were infected with 80 HAU/ml NDV for 1 h and monitored by time-lapse microscopy every 20 min. (A) Fluorescence images of subcellular localization of IRF-7-CFP (left column) and p65-YFP (right column) at denoted time post infection. The kinetics show relative nuclear fluorescence for IRF-7-CFP (cyan) and p65-YFP (yellow) of two different cells. (B) Initial nuclear translocation of p65-YFP and IRF-7-CFP were determined in 65 individual cells and plotted against each other. Colored dots represent the frequency of data points. (C, D) Heterogeneous transcription factor activation and IFN expression in single cells. Dual reporter cells expressing IRF-7-CFP together with IFN- β -tGFP were infected with 80 HAU/ml NDV and monitored by time-lapse microscopy at 20 min intervals. (C) Fluorescence images of subcellular localization of IRF-7-CFP (left column) and IFN- β -tGFP (right column) at given time post infection. The kinetics show relative fluorescence intensity for nuclear IRF-7-CFP (cyan) as well as tGFP (green) of one cell. T_{sig} indicates the signaling delay from viral infection to IRF-7 nuclear translocation and T_{gen} defines the period of time between nuclear translocation of IRF-7 and onset of IFN- β -tGFP expression. (D) Initial nuclear translocation of IRF-7-CFP (T_{sig}) and IFN- β -tGFP expression ($T_{sig} + T_{gen}$) were determined in 315 individual cells and plotted against each other. Colored dots represent the frequency of data points. (Experiments by U. Rand, M. Köster and H. Hauser)

and IFN- β expression are sources of heterogeneity in single cells.

The phenomenon of cell-to-cell variability is widely studied in many different research areas (Raser and O'Shea (2005), Maheshri and O'Shea (2007), Raj and van

2 Stochastic modeling predicts paracrine propagation of the IFN response

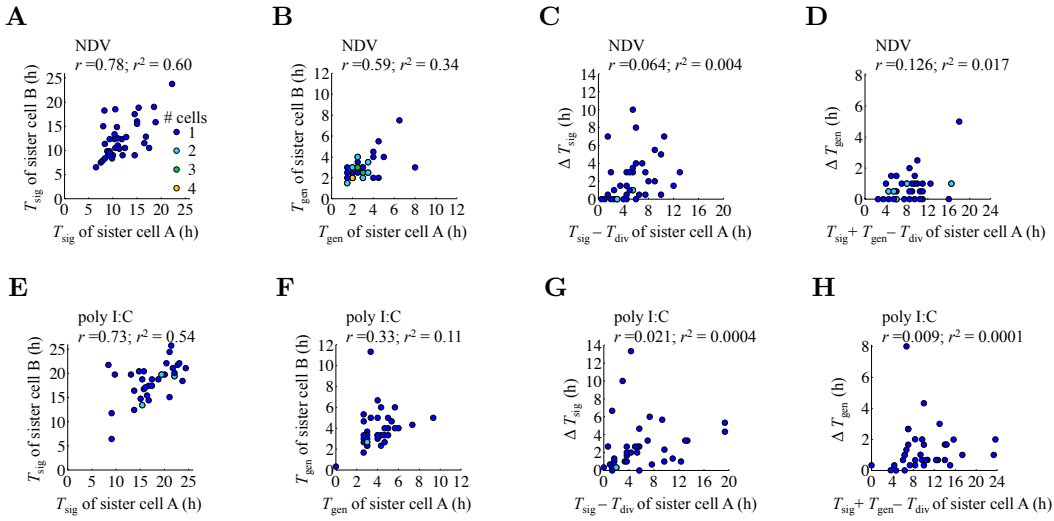


Figure 2.5: Heterogeneous IFN induction in sister cells. (A-H) Dual reporter cells expressing IRF-7-CFP or IRF-7-TagRFP (red fluorescent protein tag) together with IFN- β -tGFP were infected with 80 HAU/ml NDV for 1 h (A-D, 38 sister-cell pairs) or transfected with poly I:C (5mg/ml) (E-H, 36 sister-cell pairs) and monitored by time-lapse microscopy every 20 min. Colored dots represent the frequency of data points. Experiment-related correlation coefficient (r) and the coefficient of determination (r^2) are given at the top. (A, E) Time of IRF-7 nuclear translocation (T_{sig}) of sister cell A versus sister cell B. (B, F) Time interval between IRF-7 nuclear translocation and IFN- β -tGFP expression (T_{gen}) of sister-cell pairs. (C, G) Time elapsed from cell division (T_{div}) to IRF-7 nuclear translocation (T_{sig}) of one sister cell versus time differences between sister cells regarding IRF-7 signaling (ΔT_{sig}). (D, H) Time elapsed from cell division to IFN- β -tGFP expression ($T_{\text{sig}} + T_{\text{gen}} - T_{\text{div}}$) of one sister cell versus time differences between sister cells regarding IFN- β -tGFP expression (ΔT_{gen}). (Experiments by U. Rand, M. Köster and H. Hauser)

Oudenaarden (2008), Snijder and Pelkmans (2011)) and classified into intrinsic noise arising from inherent stochastic biochemical reactions and extrinsic noise, which results from extrinsic factors like differences in cell-cycle stage or cellular environment (Elowitz et al. (2002), Swain et al. (2002)). To analyze the origin of the single-cell heterogeneity in our system more closely, we reduced extrinsic fluctuations through examining sister cells which divided during the first hour post infection (Spencer et al. (2009)). To quantify the relation of sister cells we used besides the correlation coefficient (r) also the coefficient of determination (r^2). The value of the coefficient of determination can be interpreted as the percentage of the variation that is explained through the correlation between the sister cells (Taylor (1990)). In the experiments we observed that the virus-induced nuclear translocation of IRF-7 in sister cells happened mainly asynchronously with a temporal difference larger than 2 h in $\sim 50\%$ of the cell pairs (Figure 2.5A). An even lesser relation between sister cells was found for the time of IFN- β -tGFP expression after transcription factor activation (Figure 2.5B), which agrees with the previously described stochastic transcription of the IFN- β gene (Apostolou and Thanos (2008)). The corresponding coefficient of determination was 0.6 for T_{sig} and 0.34 for T_{gen} , which in turn means that 40% of the variability in signaling and 66% of the variability in IFN- β -tGFP expression are uncorrelated between sister cells and thus provide an estimate for the cell-intrinsic heterogeneity. In order to verify whether different viral replication kinetics in sister-

2.1 Experimental study of the IFN system revealed multi-layered stochasticity

cell pairs are a source of stochasticity, we repeated the sister cell analysis with poly I:C stimulated reporter cells. Even after transfection with poly I:C the sister cells showed a largely uncorrelated IRF-7 activation as well as IFN- β -tGFP expression (Figure 2.5E and F), with similar coefficients of determination ($r^2 = 0.54$ for T_{sig} and $r^2 = 0.11$ for T_{gen}) as after viral infection. In addition we tested if the time of cell division (T_{div}) influences the variability between sister cells. For this purpose, we considered the time elapsed since cell division versus the time differences between sister cells regarding IRF-7 signaling (ΔT_{sig}) and IFN- β -tGFP expression (ΔT_{gen}) (Figure 2.5C and D for NDV infection; Figure 2.5G and H for poly I:C stimulation). The consideration of cell division yielded very weak correlations which argues against strong impact of the cell cycle on the stochasticity in IFN induction.

In summary, our data revealed two sources of cell-to-cell heterogeneity in IFN induction, namely the virus-induced signal transduction and the subsequent IFN expression (cf. Figure 2.4). According to the sister-cell analysis, approximately half of the stochasticity in both sources can be attributed to cell-intrinsic variability (cf. Figure 2.5).

2.1.3 IFN target gene induction is an all-or-nothing switch

The observation that many cells with replicating virus do not express IFN- β or do so only very late after infection implies an incomplete virus-induced IFN- β expression (cf. Figure 2.3). To understand the functional consequences of this stochastic and not maximal IFN induction, the cellular antiviral response to IFN in terms of ISG expression should also be considered. In the literature we can find quantitative studies of IFN-stimulated signaling which have modeled relevant dynamics at cell-population level (Maiwald et al. (2010)) and regarded effects of single cell variation (Levin et al. (2011)), but without characterization of ISG expression in individual cells. To investigate IFN response at single-cell level, we stimulated our IRF-7-mCherry reporter cells (cf. section 2.1.1) with IFN- β (given in units per milliliter

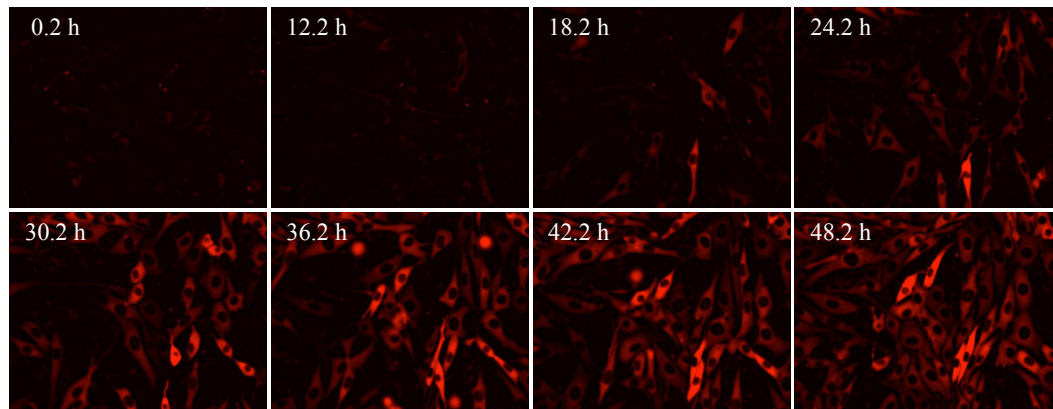


Figure 2.6: Single-cell heterogeneity of IRF-7 expression in response to IFN- β . IRF-7-mCherry reporter cells were stimulated with 500 U/ml IFN- β and detected by time-lapse microscopy at 30 min intervals. Selected fluorescence pictures at indicated time post stimulation are presented. (Experiments by U. Rand, M. Köster and H. Hauser)

2 Stochastic modeling predicts paracrine propagation of the IFN response

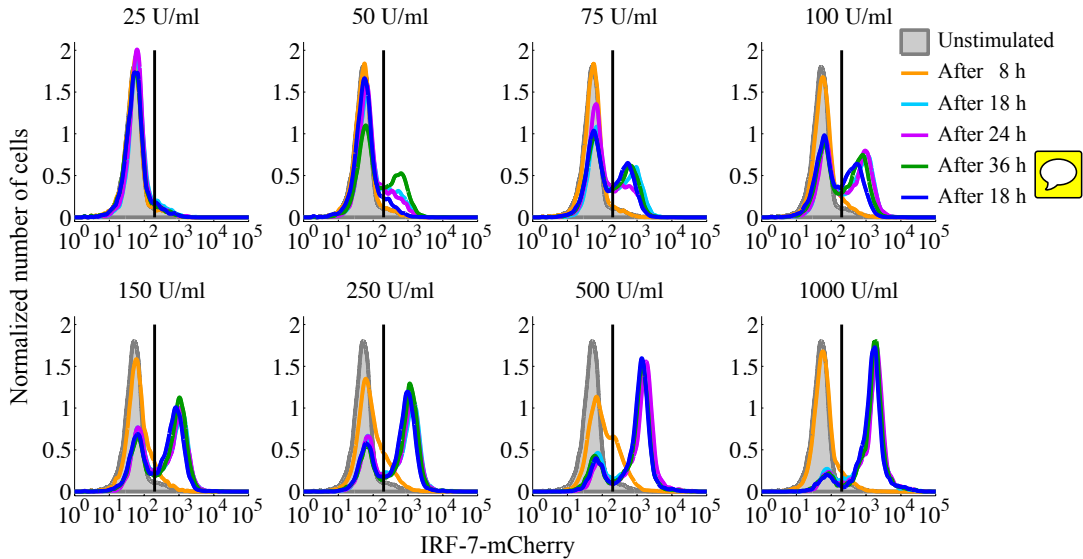


Figure 2.7: Binary time- and dose-dependent IRF-7-mCherry response towards IFN- β . IRF-7-mCherry reporter cells were stimulated with increasing concentrations of IFN- β indicated at the top of each panel. The intensity of IRF-7-mCherry expression was measured by flow cytometry at multiple time points after stimulation, which is represented through different colors. Normalized distributions are shown to enable the comparison of individual measurements with each other. (Experiments by U. Rand, M. Köster and H. Hauser)

(U/ml)) and monitored IRF-7 expression by time-lapse microscopy (Figure 2.6 and Rand, Rinas et al. (2012): Supplementary Movie S2). Surprisingly, individual cells responded very heterogeneously at various time points to IFN- β stimulation.

To quantify the observed stochastic response to IFN, IRF-7-mCherry reporter cells were stimulated with different concentrations of IFN- β and subjected to flow cytometry at several times after stimulation (Figure 2.7). The distributions of IRF-7-mCherry levels from individual cells showed a digital pattern with distinct IRF-7 expressing and non-expressing subpopulations. The IRF-7 expressing subpopulation increased with the passage of time and higher amount of extracellular IFN- β , which implies a time- and dose-dependent response to IFN. The binary IRF-7 expression was consistently measured for several IRF-7-mCherry clones (Rand, Rinas et al. (2012): Supplementary Figure S8). The unresponsiveness was not influenced by competition of cells with IFN- β , since IFN- β was still detectable in the supernatant for more than 30 h (Rand, Rinas et al. (2012): Supplementary Figure S9).

To test whether activation of IRF-7-mCherry correlates with the expression of endogenous ISGs, we separated IRF-7-mCherry negative and positive cells by fluorescence-activated cell sorting (FACS) and analyzed isolated RNA from these cells by quantitative polymerase chain reaction (qPCR) for the expression of common ISGs (Figure 2.8A). All tested ISGs showed enhanced mRNA levels in IRF-7-mCherry expressing cells (Figure 2.8A red bars, whereas the 40S ribosomal protein S9 (RPS9) serves as control). These measurements suggest that a distinct subpopulation of cells which can be identified by IRF-7-mCherry expression coordinately expresses an antiviral gene program. To examine this further, we pre-treated IRF-7-mCherry

2.1 Experimental study of the IFN system revealed multi-layered stochasticity

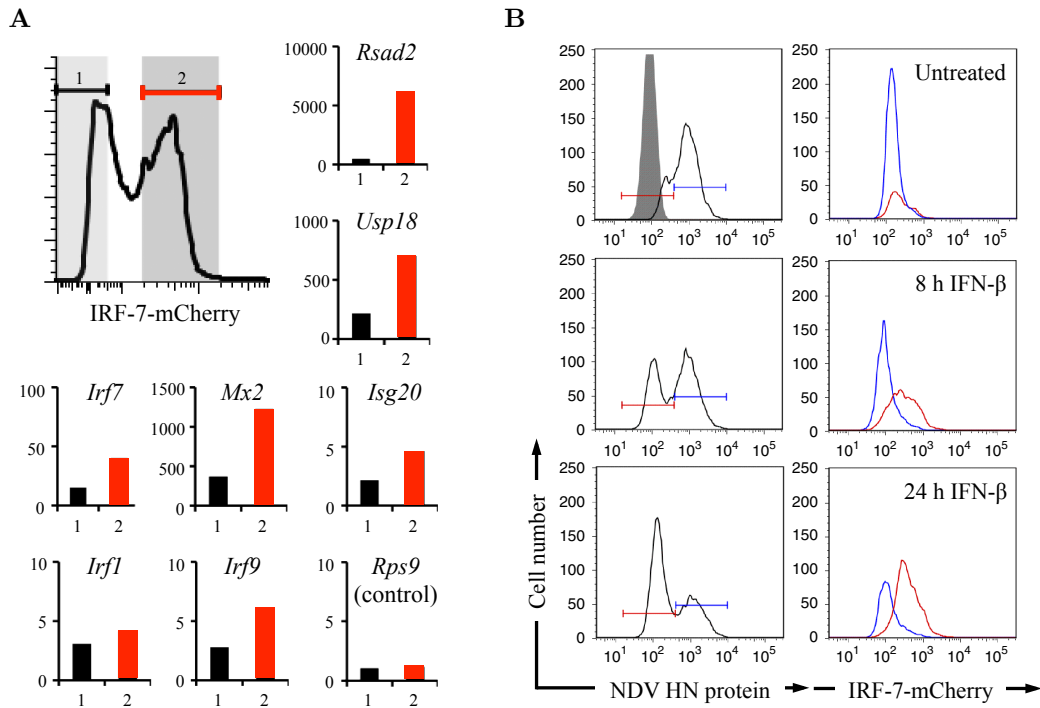


Figure 2.8: Bimodality of IRF-7 expression is reflected in ISG transcription and antiviral protection. (A) IRF-7 expression represents production of ISGs. IRF-7-mCherry reporter cells were stimulated with 500 U/ml IFN- β for 16 h and subjected to FACS. IRF-7-mCherry negative (1, black) as well as positive (2, red) cells illustrated by the shaded areas were separated. RNA was isolated from both subpopulations and analyzed by qPCR for the expression of indicated ISGs and *Rps9* as a control. The bar charts show the fold RNA increase in relation to untreated reporter cells after normalization to β -actin mRNA. (B) IRF-7 expression is correlated with antiviral protection. IRF-7-mCherry reporter cells were left untreated (upper row) or pre-treated with 500 U/ml IFN- β for 8 h (middle row) as well as 24 h (lower row) and subsequently infected with 80 HAU/ml NDV. 20 h post infection, we identified NDV HN positive (colored in blue) as well as negative cells (colored in red) (left column, intracellular antibody staining) and analyzed these two groups for IRF-7-mCherry expression (right column) by flow cytometry. (Experiments by U. Rand, M. Köster and H. Hauser)

reporter cells with IFN- β for 8 or 24 h to allow induction of ISGs and subsequently infected the cells with NDV (Figure 2.8B). Virus replicated in IRF-7-mCherry negative cells (Figure 2.8B in blue color) but not in the IRF-7-mCherry positive cells (Figure 2.8B in red color). Thus, only IRF-7-mCherry expressing cells have been protected by IFN.

Taken together, our data demonstrate that IFN response is a stochastic, IFN- β concentration-dependent, switch in individual cells. This switch is characterized by the all-or-nothing principle, in which virus can replicate in the non-responding subpopulation and the responding subpopulation is protected against viral replication.

2.2 Stochastic model of the IFN response against viral infection

The experimental study of the IFN system revealed a remarkable heterogeneity of IFN induction (cf. section 2.1.2) and subsequent antiviral IFN response (cf. section 2.1.3). To understand the stochastic dynamics of the IFN system we developed a multi-scale mathematical model that combines the virus-induced IFN signaling in individual cells with the extracellular cell-to-cell communication via secreted IFN in an infected cell population (cf. Figure 2.10). The stochastic state transitions of individual cells with respect to virus replication, IFN induction and expression of ISGs by IFN were iterated using Gillespie's algorithm (Gillespie (1976), Gillespie (1977)).

The stochastic simulation algorithm (SSA) by Daniel T. Gillespie is a Monte Carlo procedure to simulate numerically stochastic kinetics (Gillespie (2007)). The SSA is fully equivalent to the master equation approach, which in turn is the fundamental description of stochastic processes (McQuarrie (1967), Matheson et al. (1975)). Using Gillespie's algorithm enables the realization of a continuous-time Markov process (Gillespie (1976), Banks et al. (2011)), whereas the transition rate to change from one state to another is defined by the corresponding propensity function w .

A general continuous-time stochastic process $\{X(t), t \in T\}$ is a set of random variables X at time t on a time interval $T \subseteq \mathbb{R}$, whereas $X(t)$ can be in state $S_k(t)$, $k \in \mathbb{N}$. $\{X(t), t \in T\}$ is called a Markov process, if the Markov property

$$\begin{aligned} & P(X(t_{n+1}) = S_k(t_{n+1}) | X(t_0) = S_k(t_0), X(t_1) = S_k(t_1), \dots, X(t_n) = S_k(t_n)) \\ & = P(X(t_{n+1}) = S_k(t_{n+1}) | X(t_n) = S_k(t_n)) \end{aligned} \quad (2.1)$$

for successive times $t_0 \leq t_1 \leq \dots \leq t_n \leq t_{n+1}$, $n \in \mathbb{N}$, is fulfilled (Waldmann and Stocker (2004)). The used term $P(A|B)$ denotes the conditional probability of A under the condition B . The Markov property therefore requires a memoryless system in which a state change depends only on the current state and not on the past history.

For our model we initially consider a cell population of N cells. Since the experimentally used virus cannot spread (cf. section 2.1.2 page 5), we restrict the viral activity in our model to the initial infection with subsequent virus replication and neglect reinfection. Depending on the initial infection dose, we set a fraction of cells as infected. A certain percentage of these infected cells will eventually express IFN- β according to the measured number of IFN- β -tGFP $^+$ cells (cf. Figure 2.3). Since the MOIs used in the experiments are approximately unity or below, the number of infecting virus particles per cell is low. As initial condition we therefore randomly assign each cell $i = 1, \dots, N$ a number of intracellular virus particles V_i according to

$$V_i(0) = \begin{cases} 0 & , \text{if cell } i \text{ is uninfected;} \\ p \in \{1, 2, 3\} & , \text{if cell } i \text{ is infected.} \end{cases} \quad (2.2)$$

The replication of virus particles is modeled as a birth-death process (Kendall (1949)) with the rate constant of virus replication r_V and the rate constant of virus

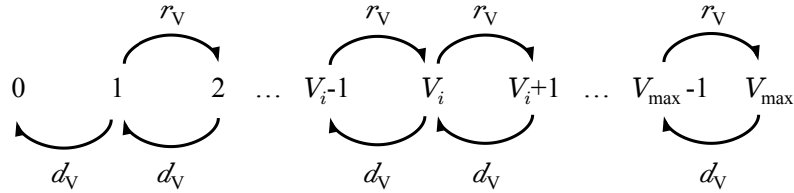


Figure 2.9: Scheme of the used birth-death process to simulate virus replication. Intracellular virus particles V_i replicate in an infected cell $i \in \{1, \dots, N\}$ with the rate constant of virus replication r_V . The maximal number of virus particles which an intact cell can harbor is defined by V_{\max} . The antiviral effect of ISG expression inhibits further viral replication and decreases the intracellular viral load with the rate constant of virus decay d_V .

decay d_V (Figure 2.9). The associated propensity function of virus replication is specified through

$$w_{V,i}^+ = r_V V_i \mathcal{H}(V_{\max} - V_i), \quad (2.3)$$

whereas the Heaviside step function (Werner (2005))

$$\mathcal{H}(V_{\max} - V_i) = \begin{cases} 0 & , \text{ if } V_i \geq V_{\max}; \\ 1 & , \text{ if } V_i < V_{\max} \end{cases} \quad (2.4)$$

was chosen to account for the limited capacity of an intact cell to harbor maximal V_{\max} virus particles.

The investigation of the virus-induced IFN expression detected two sources of single-cell variability, firstly, the activation of latent transcription factors NF- κ B and IRF-7 downstream of viral sensing by RIG-I (cf. Figure 2.4A and B) and, secondly, induction of the IFN- β gene by nuclear located NF- κ B and IRF-7 (cf. Figure 2.4C and D). Based on the sister-cell analysis, both of these sources arise substantially from cell-intrinsic noise (cf. Figure 2.5). Thus, we attributed cell-to-cell variability in the model to intrinsic stochasticity in both kinds of processes. The onset of transcription factor activation and IFN- β expression are broadly distributed among the cell population (cf. Figure 2.4D). But the examination of single-cell kinetics in terms of nuclear fluorescence intensity of the transcription factors NF- κ B as well as IRF-7 (cf. sample trajectories in Figure 2.4A) and IFN- β fluorescence (cf. sample kinetics in Figure 2.4C) show a quantitatively steep rise once nuclear translocation and gene induction, respectively, have been triggered. To account for the switch-like activation of the transcription factors and subsequent IFN- β expression, we describe the dynamics of these events in an individual cell $i = 1, \dots, N$ as stochastic transitions between discrete states (virus-infected, NF- κ B/IRF-activated, IFN- β expressing along the vertical axis in Figure 2.10) (Mariani et al. (2010)). The chosen propensity function of transcription factor activation triggered by virus replication

$$w_{TF,i}^+ = k_{RIG-I} \frac{V_i^{h_V}}{K_V^{h_V} + V_i^{h_V}}, \quad (2.5)$$

corresponds to a Hill function (Alon (2006)) with the half-saturation constant K_V , the Hill coefficient h_V and the rate k_{RIG-I} of RIG-I pathway activation by virus. This formulation enables a threshold response of the RIG-I pathway with saturation regarding the number of intracellular virus particle. Since some reporter cells

2 Stochastic modeling predicts paracrine propagation of the IFN response

demonstrated that in the nucleus accumulated IRF-7 also returns to the cytoplasm (cf. left column in Figure 2.4A, Rand and Hauser (2010)), we allow in our model the inactivation of the RIG-I pathway with the rate

$$w_{\text{TF},i}^- = l_{\text{RIG-I}}. \quad (2.6)$$

The nuclear translocation of the transcription factors NF- κ B as well as IRF-7 lead to IFN- β gene induction according to the transition rate

$$w_{\text{I},i}^+ = k_{\text{IFN}}, \quad (2.7)$$

whereas IFN- β expression can also terminate with the rate constant

$$w_{\text{I},i}^- = l_{\text{IFN}}. \quad (2.8)$$

The experimental data show that the fraction of IFN- β expressing cells determines the extracellular concentration of IFN- β (cf. Figure 2.3C). Although extracellular IFN- β decreases through the cellular uptake and degradation in the medium, IFN- β was always detectable in the supernatant (cf. Rand, Rinas et al. (2012): Supplementary Figure S9), which indicates high molecule number of IFN- β in the cell culture. Therefore we calculate the extracellular concentration of IFN- β in parallel with the Gillespie algorithm using a deterministic, explicit Euler method. In our model, extracellular IFN- β I evolves through the secretion of IFN expressing cells with the rate constant k_S and is degraded according to the rate constant d_{IFN} . Regarding the high diffusion coefficient of IFN (Kreuz and Levy (1965): $D_{\text{IFN}} = 342000 \mu\text{m}^2/\text{h}$; Hu et al. (2011): $D_{\text{IFN}} = 108000 \mu\text{m}^2/\text{h}$) diffusion on the relevant length scale of several cell diameters occurs fast within minutes compared to the hour-timescale of IFN and ISG expression, so that we assume uniform distribution of secreted IFN.

Our studies expose the IFN response as an IFN- β concentration dependent all-or-nothing switch in individual cells (cf. Figure 2.7 and Figure 2.8). To account for this switch-like induction of antiviral ISGs, we modeled the IFN response as two stochastic transitions between discrete states consisting of the IFN-dependent nuclear translocation of STAT1/2 (Lillemeier et al. (2001), Vinkemeier (2004)) and the subsequent expression of ISGs, such as IRF-7 (cf. horizontal axis in Figure 2.10). We formulate the activation of STAT1/2 by autocrine or paracrine uptake of extracellular IFN- β I with the propensity function

$$w_{\text{STAT},i}^+ = k_{\text{STAT}} \frac{I^{h_{\text{IFN}}}}{K_{\text{IFN}}^{h_{\text{IFN}}} + I^{h_{\text{IFN}}}}, \quad (2.9)$$

where k_{STAT} , K_{IFN} and h_{IFN} denote the rate, the half-saturation constant and the Hill coefficient of STAT1/2 pathway activation by IFN, respectively.

Activated STAT1/2 in turn cause the expression of ISGs, including IRF-7, with the rate constant

$$w_{\text{ISG},i}^+ = k_{\text{ISG}}. \quad (2.10)$$

As the observed number of IRF-7 expressing cells remained high within the observation period of 48 h post infection (cf. Figure 2.11B, lowest coordinate system), we considered neither a termination of ISG expression nor an inactivation of STAT1/2.

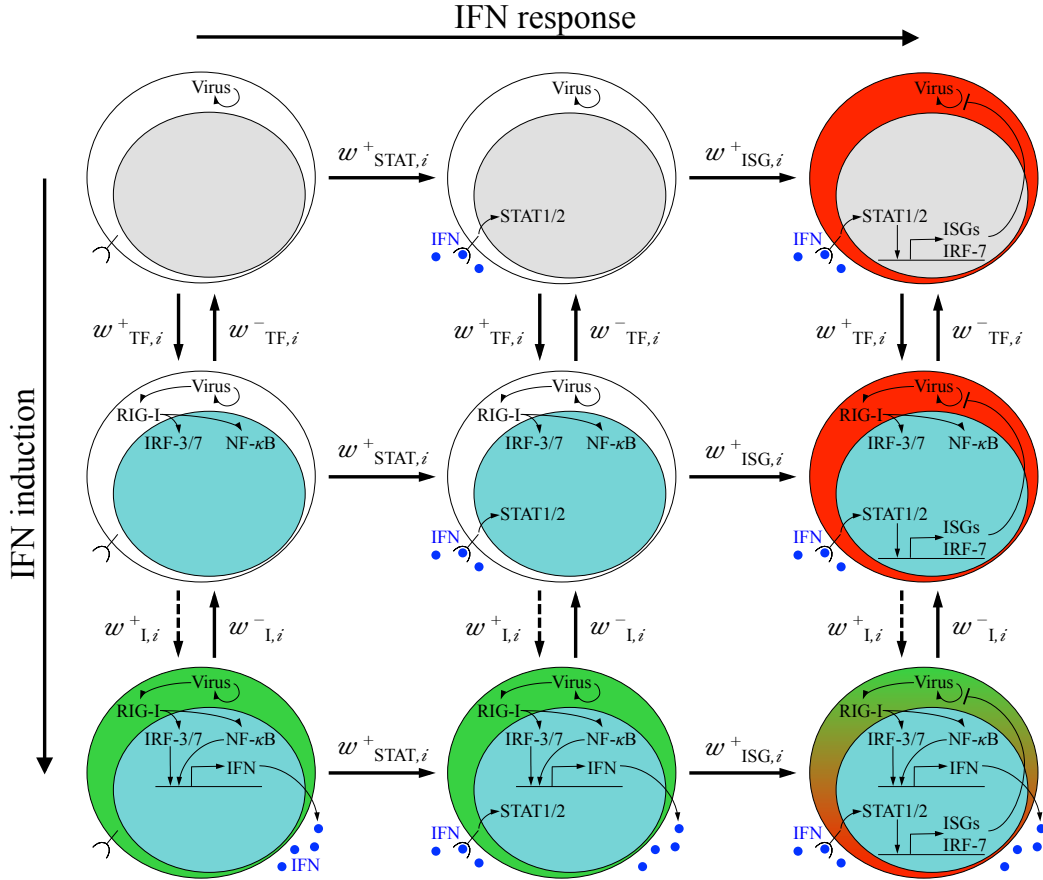


Figure 2.10: A multi-scale mathematical model of IFN induction and response. The model describes an infected cell population with state transitions of individual cells according to (i) virus replication, (ii) virus-induced nuclear translocation of the transcription factors IRFs/NF- κ B (cyan nucleus), (iii) IFN- β gene induction (green cytoplasm), (iv) nuclear translocation of STAT1/2 by extracellular IFN and (v) expression of antiviral ISGs including IRF-7 (red cytoplasm), in combination with the cell-to-cell communication via secreted IFN. Possible state changes of an individual cell $i \in \{1, \dots, N\}$ depend on the propensity functions w_i^\pm . The color code corresponds to the experimentally used fluorescence reporter cells (cf. section 2.1.1). Induction of IFN- β (dashed arrow) is explicitly modeled as a multi-step process to fit the available experimental data (cf. section 2.4.2); all other state transitions are modeled as single steps (solid arrows).

To characterize the induction of an antiviral state through IFN response, we assume that in an ISG expressing cell $i \in \{1, \dots, N\}$ viral replication is inhibited and the intracellular viral load V_i declines according to the propensity function

$$w_{V,i}^- = d_V V_i, \quad (2.11)$$

whereas d_V terms the rate constant of virus decay (cf. Figure 2.9).

An additional overall decline of viral load can be attributed to the death of virus-infected cells (cf. decrease of HN $^+$ cells in Figure 2.3A and B, orange color). To keep the model as simple as possible we have neglected cell death and also cell proliferation by simulating a constant cell population. The consideration of a non-

2 Stochastic modeling predicts paracrine propagation of the IFN response

growing cell population is justified since we did not detect obvious differences in heterogeneous IFN- β induction between the cell fraction dividing during the time of observation (cf. Figure 2.5A and B) and the whole cell population which contains a sizable proportion of non-dividing cells (cf. Figure 2.4B and D).

2.3 Model simulations based on Gillespie's algorithm

The simulations of our cell population model (cf. Figure 2.10), which couples the stochastic state changes of individual cells according to the propensity functions $w_{\cdot,i}^{\pm}$ (cf. section 2.2) with the deterministic iteration of extracellular IFN- β were performed using Gillespie's direct method.

To execute a time step of the dynamics, we considered at time t all possible state changes of each cell $i = 1, \dots, N$ and calculated the time interval dt after which the next stochastic switching event takes place by

$$dt = -\frac{\ln(u_1)}{w_0}, \quad (2.12)$$

where u_1 denotes an uniformly distributed random number. The denominator in (2.12) is defined as

$$\begin{aligned} w_0 &= \sum_{s \in \mathcal{S}^+} \sum_{i=1}^N w_{s,i}^+ + \sum_{s \in \mathcal{S}^-} \sum_{i=1}^N w_{s,i}^- \\ &= \sum_{k=1}^M W_k \end{aligned} \quad (2.13)$$

with $\mathcal{S}^+ = \{\text{V, TF, I, STAT, ISG}\}$ as well as $\mathcal{S}^- = \{\text{V, TF, I}\}$ a  represents the sum of all propensity functions W_k for $k = 1, \dots, M$ that “lead away” from the current state of the system.

The actually occurring state transition W_j at time $t + dt$ has to fulfill the condition

$$\sum_{k=1}^{j-1} W_k < u_2 w_0 \leq \sum_{k=1}^j W_k, \quad (2.14)$$

whereas u_2 terms a second uniformly distributed random number.

In parallel to the Gillespie algorithm, the extracellular IFN- β concentration I is computed through

$$I(t + dt) = I(t) + dt[k_S N_{\text{IFN}}(t) - d_{\text{IFN}} I(t)], \quad (2.15)$$

where $N_{\text{IFN}}(t)$ stands for the number of IFN- β expressing cells at time t . After transforming the equation (2.15)

$$\frac{I(t + dt) - I(t)}{dt} = k_S N_{\text{IFN}}(t) - d_{\text{IFN}} I(t)$$

2.3 Model simulations based on Gillespie's algorithm

$$\begin{aligned} \iff & \frac{dI}{dt} = k_S N_{\text{IFN}}(t) - d_{\text{IFN}} I(t) \\ \iff & I = k_S N_{\text{IFN}} - d_{\text{IFN}} I \end{aligned} \quad (2.16)$$

~~it becomes apparent that~~ we used the discrete Euler approximation of the differential equation (2.16), whereas the time step dt needs to be sufficiently small to satisfy $dt \ll d_{\text{IFN}}^{-1}$. We found the latter condition to be guaranteed with the parameter choices (cf. Table 2.1) for our model.

After every Gillespie step, we updated the system in accordance with the current states of the cells. To compare the model simulations with the experimental data (Figure 2.11), we used the following readouts (ROs):

- (RO1) The total viral load of the cell population given by

$$V(t) = \sum_{i=1}^N V_i(t). \quad (2.17)$$

A direct comparison of the simulated amount of virus particles with the measured mean fluorescence intensity of the HN staining (cf. Figure 2.3A) was enabled with an appropriate scaling factor.

- (RO2) The initial nuclear translocation times of the transcription factors NF- κ B and IRF-7 after infection $T_{\text{sig},i}, i = 1, \dots, N$, to fit the imaged activation times of the transcription factors T_{sig} in the corresponding reporter cells (cf. Figure 2.4D, explicit for IRF-7 and analog for NF κ -B as both transcription factors synchronously translocate into the nucleus (cf. Figure 2.4B)).
- (RO3) The time delays between transcription factor activation and onset of IFN- β expression $T_{\text{gen},i}, i = 1, \dots, N$, for the estimation of the visualized IFN- β -tGFP switching-on times after activation of the transcription factors T_{sig} in the dual IRF-7-CFP/IFN- β -tGFP reporter cells (cf. Figure 2.4D).
- (RO3) The number of IFN- β expressing cells at time t $N_{\text{IFN}}(t)$, which relates to the monitored IFN- β -tGFP $^+$ reporter cells (cf. Figure 2.3B).
- (RO4) The extracellular IFN- β concentration over time $I(t)$.
- (RO5) The number of ISG expressing cells at time t $N_{\text{ISG}}(t)$, which represents the investigated IRF-7-mCherry $^+$ reporter cells (cf. Figure 2.7).

For the parameterization of our model, we focused on the extensive data for high-dose infections with 40 and 80 HAU/ml NDV (Figure 2.11; Table 2.1; section 2.4). Fitting of the observed distributions regarding the NF- κ B/IRF-7 nuclear translocation times (T_{sig}) and the IFN- β -tGFP switching-on times ($T_{\text{sig}} + T_{\text{gen}}$) results in a good approximation of the data (Figure 2.11A) and enables the description of the measured kinetic of IFN- β -tGFP $^+$ cells (Figure 2.11B, second coordinate system). The fit concerning the IFN induction required that (i) the activation of the RIG-I-mediated signaling by virus is cooperative (cf. section 2.4.1) and (ii) IFN- β gene induction is modeled as a multi-step process (cf. section 2.4.2). These two conclusions drawn from the parameter estimation corresponds well with experimental

2 Stochastic modeling predicts paracrine propagation of the IFN response

findings from the literature (Onoguchi et al. (2010), Ford and Thanos (2010)).

To estimate the parameters of the IFN response, we initially scaled our model to the measuring unit of IFN by fitting the dose-response curve of IRF-7-expressing cells depending on external IFN- β (cf. Figure 2.14). Restricted through this calibration and the already specified dynamics of IFN- β producing cells (cf. Figure 2.11B, green curve), we determined the IFN- β secretion rate per cell to match the observed time course of extracellular IFN (cf. Figure 2.11B, third coordinate system). With these parameters (cf. Table 2.1), the simulated kinetics of IRF-7-expressing cells agreed with the data (cf. Figure 2.11B, lowest coordinate system).

Importantly, the model simulations demonstrate that the single cell heterogeneity of transcription factor activation, IFN- β gene induction as well as ISG expression translates into predictable dynamics of IFN-secreting and protected cell fractions at the population level.



Model parameter	Symbol	Value
Maximum viral load per cell	V_{\max}	130
Rate constant of virus replication	r_V	0.34/h
Rate constant of virus decay	d_V	0.1/h
Rate of RIG-I pathway activation by virus	$k_{\text{RIG-I}}$	0.48/h
Rate of RIG-I pathway inactivation	$l_{\text{RIG-I}}$	0.4/h
Half-saturation constant of RIG-I pathway activation by virus	K_V	43
Hill coefficient of RIG-I pathway activation by virus	h_V	3
Rate constant of IFN- β gene induction	k_{IFN}	1.79/h
Rate of termination of IFN- β expression	l_{IFN}	0.08/h
Rate constant of IFN- β secretion	k_S	0.13 U/(h ml cell)
Rate constant of IFN- β degradation	d_{IFN}	0.15/h
Rate of STAT1/2 pathway activation	k_{STAT}	0.1/h
Half-saturation constant of STAT1/2 pathway activation by IFN- β	K_{IFN}	100 U/ml
Hill coefficient of STAT1/2 pathway activation by IFN- β	h_{IFN}	1
Rate constant of ISG (IRF-7) induction by STAT1/2 pathway	k_{ISG}	0.1/h

Table 2.1: Model parameters of the stochastic model. Based on the biological meaning of the model parameters (cf. section 2.2), we determined the parameter values as depicted in section 2.4. All model simulations in sections 2.3 and 2.5 refer to this parameter set.

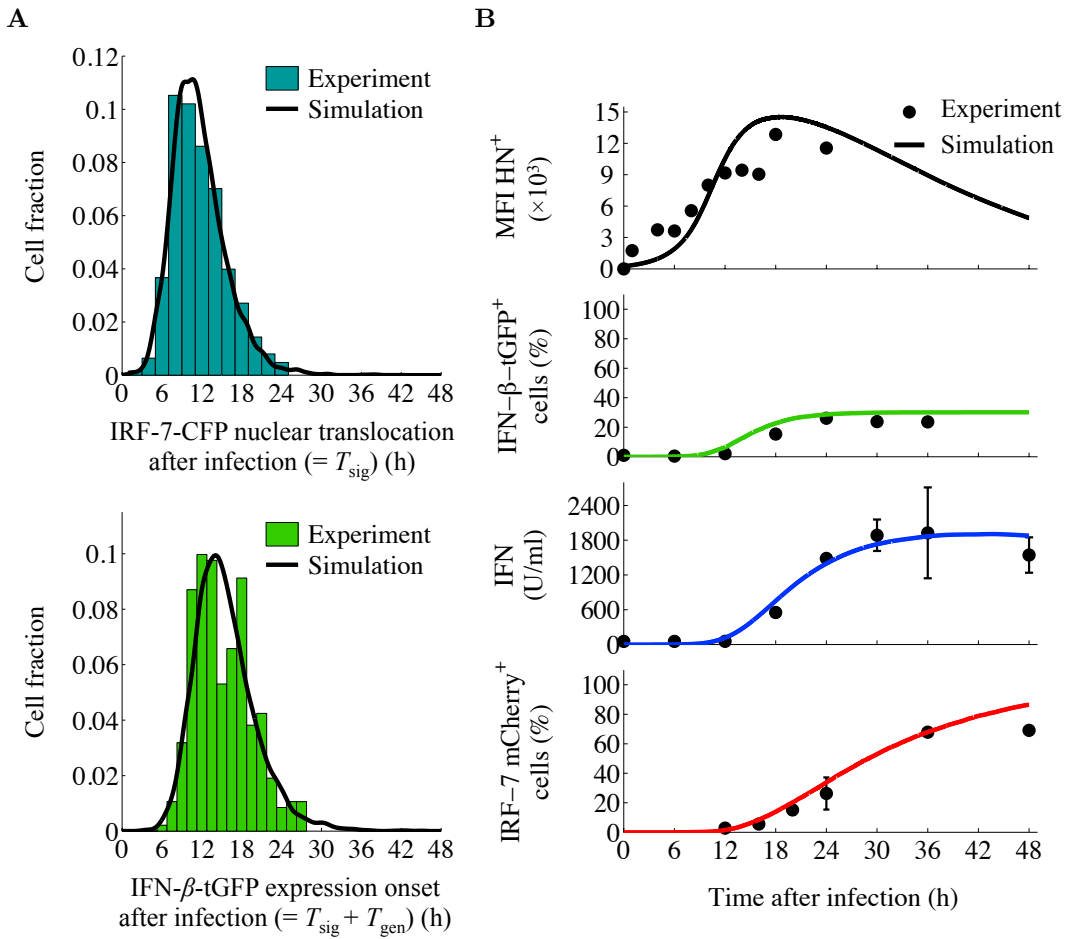


Figure 2.11: Simulating the multi-layered cell-to-cell heterogeneity of the IFN system results in predictable populations dynamics. (A) Model simulations of NF- κ B/IRF nuclear translocation time points and IFN- β -tGFP onset times versus experimental data. With the stochastic model computed distributions (black lines) match the data of IRF-7-CFP nuclear translocation times (T_{sig} , cyan histogram) and IFN- β -tGFP expression onset ($T_{\text{sig}} + T_{\text{gen}}$, green histogram) monitored in single cells after infection with 80 HAU/ml NDV (cf. Figure 2.4D for a representation of individual time points). (B) Comparison between simulated and measured cell population dynamics for high-dose NDV infection. The stochastic model reproduces the observed kinetics of viral load (as measured by HN expression), IFN- β -tGFP induction, extracellular IFN titre and IRF-7-mCherry expression (solid lines, model; dots, experimental data; infection dose 40 HAU/ml NDV). The smooth model curves in (A) and (B) are mean values obtained by simulating 10^4 cells. (Experiments by U. Rand, M. Köster and H. Hauser)

2.4 Estimation of model parameters

The Gillespie algorithm is a prevalent and valuable method to simulate stochastic processes. Nevertheless, the long computation time of this algorithm for extensive models with large time scales is a serious disadvantage (Gillespie (2007), Cao and Samuels (2009), Banks et al. (2011)). Also the simulation of our full model for a sufficient number of cells ($N = 10^4$ cells) of several hours is very time consuming and practically excludes straightforward optimization approaches for parameter estimation. Therefore we divided the parameter estimation problem into three parts: (1) determination of parameters for the virus-induced activation of the transcription factors IRFs/NF- κ B (cf. section 2.4.1), (2) identification of parameters with respect to IFN- β expression (cf. section 2.4.2) and (3) estimation of parameters concerning the IFN response (cf. section 2.4.3). 

The first two parts consider the induction of IFN in individual cells without cell-to-cell communication via secreted IFN- β . As the simulation of isolated single cell behavior is much faster than the complete model, rigorous parameter estimation is applicable and several mechanistically relevant conclusions will be drawn from these calculations.

The third part regarding ISG induction depends on the intercellular signaling between cells, which implies the need for simulating large numbers of cells and thus having impractically long calculation times. However, it turns out that we can still derive quantitative features of ISG expression from the experimental data.

An overview of the determined parameter values in this section is provided in Table 2.1 and serves as a reference for the used parameter set of all model simulations in sections 2.3 and 2.5.

2.4.1 Parameter determination for the virus-induced activation of the transcription factors of IFN

In our model, we describe the activation of the transcription factors of IFN in an infected cell $i \in \{1, \dots, N\}$ as a state change from virus-infected to NF- κ B/IRF-activated by the propensity function

$$w_{TF,i}^+ = k_{RIG-I} \frac{V_i^{hv}}{K_V^{hv} + V_i^{hv}},$$

with the rate constant k_{RIG-I} , the half-saturation constant K_V and the Hill coefficient h_V of RIG-I pathway activation depending on the intracellular viral load V_i (cf. Figure 2.10). A perfectly suited experiment to determine the parameters of $w_{TF,i}^+$ is the single cell analysis of the nuclear translocation time of NF- κ B and IRF-7 after infection T_{sig} monitored by live-cell imaging (cf. Figure 2.4D explicit for IRF-7 and analog for NF- κ B as both transcription factors synchronously translocate into the nucleus (cf. Figure 2.4B)). To determine computationally this measured histogram of the nuclear translocation times of the transcription factors (Figure 2.12A), we utilize a submodel comprising viral replication and subsequent NF- κ B/IRF-7 activation.

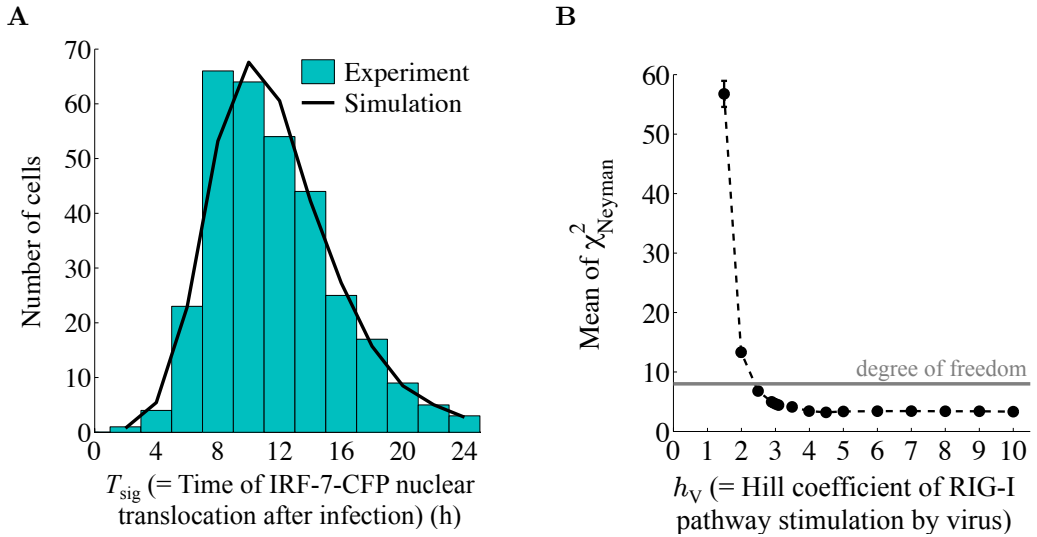


Figure 2.12: Parameter determination demonstrates a cooperative induction of RIG-I mediated signaling by virus. (A) Parameter estimation of virus-induced transcription factor activation. As basis for the parameter determination serves the initial nuclear translocation time of IRF-7 monitored by live-cell imaging in 315 IRF-7-CFP reporter cells after infection with 80 HAU/ml NDV (cyan histogram, cf. Figure 2.4D for a representation of individual time points). The computed distribution (black line) is obtained by simulating 5×10^4 runs of the mathematical submodel comprising viral replication and subsequent NF- κ B/IRF-7 activation. A match of the computed with the measured distribution was achieved under the usage of the simulated annealing algorithm (Experiments by U. Rand, M. Köster and H. Hauser). (B) Profile likelihood with respect to the Hill coefficient of virus-induced RIG-I signaling h_V . The profile likelihood calculation was repeated 100 times for each fixed value of h_V . Shown are the resulting mean values and standard deviations of Neyman's chi-squares statistic. The upper limit for a good fit is defined by the degree of freedom (DF = 8, cf. (2.23)).

To simulate this submodel we initially characterized viral reproduction by comparing the model with the measured time course of viral replication after high-dose infection (cf. Figure 2.11B, upper coordinate system). Accordingly, we set the rate constant of virus replication $r_V = 0.34/h$, the maximum viral load per cell $V_{\max} = 130$ and the rate constant of virus termination $d_V = 0.1/h$, which results in a satisfactory match of the model with the data 

Next, we computed the distribution of NF- κ B/IRF translocation times by simulating the submodel consisting of viral replication and subsequent NF- κ B/IRF-7 activation sufficiently often using Gillespie's algorithm. To adjust this computed distribution to the experimentally measured histogram, we allowed the parameters of the RIG-I pathway activation by virus ($k_{\text{RIG-I}}$, K_V and h_V) to vary while keeping the previously determined viral replication parameters (r_V , V_{\max} and d_V) fixed. As objective function we used Neyman's chi-squares statistic (Baker and Cousins (1984)), which considers the squared difference between the binned observed and simulated events weighted by the inverse binned experimental data:

$$\chi^2_{\text{Neyman}} = \sum_{k=1}^B \frac{(D_k - E_k)^2}{D_k}, \quad (2.18)$$

2 Stochastic modeling predicts paracrine propagation of the IFN response

with the number of bins of the histograms B , the number of observed events in the k th bin D_k and the number of simulated events in the k th bin E_k for $k \in \{1, \dots, B\}$, under the condition

$$\sum_{k=1}^B D_k = \sum_{k=1}^B E_k. \quad (2.19)$$

In order to satisfy the condition (2.19) and to ensure accuracy by simulating much more events (5×10^4 runs) than experimentally measured (315 cells), we calculated E_k under the usage of the cumulative distribution function (CDF) of the simulations for transcription factor activation at time t given by

$$\text{CDF}_{\text{TF}}(t) = \frac{1}{N_s} \sum_{i=1}^{N_s} \mathbb{1}_{[0;t]}(\mathcal{T}_{\text{sig},i}), \quad (2.20)$$

with the number of simulated events N_s , the simulated nuclear translocation times of the transcription factors $\mathcal{T}_{\text{sig},i}$, $i = 1, \dots, N_s$ and the characteristic function $\mathbb{1}$ of the interval $[0; t]$

$$\mathbb{1}_{[0;t]}(\mathcal{T}_{\text{sig},i}) = \begin{cases} 1 & , \text{ for } \mathcal{T}_{\text{sig},i} \in [0; t]; \\ 0 & , \text{ for } \mathcal{T}_{\text{sig},i} \notin [0; t] \end{cases} \quad (2.21)$$

(Königsberger (2004)). After simulating the submodel N_s times, we computed the number of simulated events in the k th bin according to

$$E_k = N_{\text{data}}(\text{CDF}_{\text{TF}}(t_k^{j+1}) - \text{CDF}_{\text{TF}}(t_k^j)), \quad (2.22)$$

where N_{data} denotes the number of observed data points, while t_k^j and t_k^{j+1} represent the left and the right bin edge of the k th bin for $j \in \{1, \dots, B\}$, respectively.

For the minimization of the objective function (2.18) we applied the simulated annealing algorithm (Schneider and Kirkpatrick (2006), Gonzalez et al. (2007)). The resulting parameter values ($k_{\text{RIG-I}} = 0.48/\text{h}$, $K_V = 43$ and $h_V = 3.0$) yield a good match of computed and measured distributions of nuclear translocation times of the transcription factors (Figure 2.12A).

From a biological point of view, the most interesting feature of this parameter set is the high Hill coefficient h_V as a Hill coefficient larger than 1 implies positive cooperativity (Murray (2002)). To analyze how robust the estimation of the Hill coefficient h_V is, we used the profile-likelihood method (Venzon and Moolgavkar (1988), Raue et al. (2009)). For this purpose, we fixed h_V systematically to different values around the estimated optimum of $h_V = 3.0$ and refitted $k_{\text{RIG-I}}$ as well as K_V by simulated annealing. To ensure that the obtained values of the objective function (2.18) are unaffected by the inherent stochasticity of the submodel, we repeated the calculation for each fixed value of h_V 10^4 times. The profile likelihood (Figure 2.12B) shows the corresponding mean values of Neyman's chi-squares statistic for each fixed h_V . A measure for the goodness of the fit is the degree of freedom (DF), which defines an upper limit for good fits (Press et al. (2007)). In the present case, the degree of freedom is calculated by

$$\begin{aligned} \text{DF} &= B - \text{normalization constraint} - \text{number of fit parameters} \\ &= 12 - 1 - 3 \\ &= 8. \end{aligned} \quad (2.23)$$

A non-cooperative activation of the RIG-I pathway ($h_V = 1$) far exceeds the degree of freedom, whereas a Hill coefficient $h_V \geq 3$ leads to a very good fit of the translocation-time distribution. Based on these findings we conclude that the activation of the RIG-I pathway by virus is cooperative, while the available data are insufficient to estimate the precise degree of cooperativity.

After the nuclear translocation of the transcription factor IRF-7 we monitored in some reporter cells a relocation of IRF-7 back to the cytoplasm and after a while again an accumulation in the cytoplasm (cf. left column in Figure 2.4A, Rand and Hauser (2010)). To account for this nucleocytoplasmic transport of IRF-7 we allow in our model the inactivation of the RIG-I pathway with the rate $l_{\text{RIG-I}}$, which consequently prevents or at least delays a subsequent IFN- β gene induction. For the adaptation of the parameter $l_{\text{RIG-I}}$, it is therefore necessary to simulate the whole IFN induction pathway with the determined parameter values for viral replication and RIG-I pathway activation explained in this section  together with the results from the parameter estimation of IFN- β gene induction in the following section 2.4.2. After simulation of the IFN induction, we compared the arising distribution of IFN- β switching-on times with the measured histogram (cf. Figure 2.11A, lower graph) and found an improved match by setting $l_{\text{RIG-I}} = 0.4/\text{h}$.

2.4.2 Parameter determination of the IFN expression

After the virus-induced nuclear translocation of the transcription factors NF- κ B and IRF-7 we detected that the majority of the cells (91% at 80 HAU/ml NDV) also induces the IFN- β gene (cf. Figure 2.4D). The time delay between nuclear translocation of IRF-7 and onset of IFN- β -tGFP expression T_{gen} varied considerably in individual cells and results in a broad distribution (Figure 2.13). To simulate the heterogeneous onset of IFN- β expression after transcription factor activation using Gillespie's algorithm, we have to formulate this state transition as a Markov process (cf. section 2.2 page 14). The only continuous distribution fulfilling the Markov property (2.1) is the memoryless exponential distribution (cf. Waldmann and Stocker (2004)). However, according to the shape of the experimentally measured histogram of T_{gen} (cf. Figure 2.13) a single exponentially distributed transition rate cannot generate the distinct time delay between transcription factor activation and IFN- β gene induction. In comparison, the distribution of transcription factor translocation times T_{sig} (cf. Figure 2.12A) can neither be modeled with a single exponential rate (cf. section 2.4.1). In this case, the time delay between virus infection and transcription factor activation is explained by the viral replication process (cf. Figure 2.9).

Explanation for the observed time delay between the nuclear translocation of the transcription factors NF- κ B/IRF-7 and IFN- β expression is the multi-step assembly of the IFN- β enhanceosome that activates transcription from the IFN- β promoter (Ford and Thanos (2010)). Therefore we analyzed if the measured histogram of T_{gen} can be fitted with a gamma distribution $\gamma(m, z)$, which describes the sum of m independent and with parameter z exponentially distributed random numbers (Press et al. (2007)). Based on the measured times of IFN- β -tGFP expression onset

2 Stochastic modeling predicts paracrine propagation of the IFN response

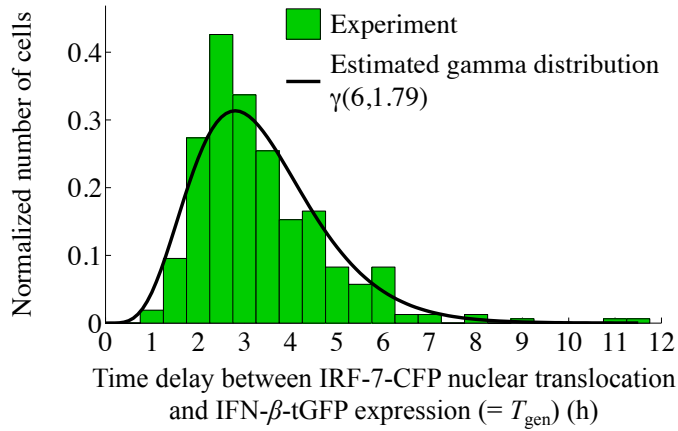


Figure 2.13: Parameter estimation characterizes IFN- β gene induction as a multi-step process. The parameter determination of IFN- β gene induction is based on the time delay between IRF-7-CFP nuclear translocation and IFN- β -tGFP expression (T_{gen}) monitored by live-cell imaging in 315 dual reporter cells after infection with 80 HAU/ml NDV (green histogram, cf. Figure 2.4D for a representation of individual time points). The observed histogram can be approximated by the gamma distribution $\gamma(6, 1.79)$ (black line), which represents a stochastic process consisting of 6 consecutive and with rate 1.79/h exponentially distributed steps. (Experiments by U. Rand, M. Köster and H. Hauser)

after transcription factor activation $T_{\text{gen},i}$ for $i = 1, \dots, N_{\text{data}}$ monitored in $N_{\text{data}} = 315$ individual cells (cf. Figure 2.13), we estimated the parameters of the gamma distribution m and z with the maximum-likelihood method (Myung (2003)). For this purpose, we have to maximize the likelihood function L of our sample $T_{\text{gen},i}$, $i = 1, \dots, N_{\text{data}}$, which is described as

$$L(p_1, \dots, p_{N_p} | T_{\text{gen},1}; \dots; T_{\text{gen},N_{\text{data}}}) = f(T_{\text{gen},1}; \dots; T_{\text{gen},N_{\text{data}}} | p_1, \dots, p_{N_p}) \quad (2.24)$$

under the usage of the assumed common density function $f(t | p_1, \dots, p_{N_p})$ with the parameters p_1, \dots, p_{N_p} . The density function of the considered gamma distribution f_γ is given $\forall m, z > 0$ by

$$f_\gamma(t | m, z) = \begin{cases} \frac{z^m}{\Gamma(m)} t^{m-1} e^{-z t} & , \text{ for } t > 0; \\ 0 & , \text{ for } t \leq 0, \end{cases} \quad (2.25)$$

with the natural exponential function $\exp(x) = e^x, \forall x \in \mathbb{C}$ and the gamma function $\Gamma(m)$. According to Euler's integral representation, the gamma function is defined for $m > 0$ as

$$\Gamma(m) = \int_0^\infty t^{m-1} e^{-t} dt. \quad (2.26)$$

Instead of maximizing L , we preferred to maximize the log-likelihood function \mathcal{L} of

our independent and identically distributed (i.i.d.) sample $T_{\text{gen},i}$, $i = 1, \dots, N_{\text{data}}$:

$$\begin{aligned}
 & \mathcal{L}(m, z | T_{\text{gen},1}; \dots; T_{\text{gen},N_{\text{data}}}) \\
 &= \ln(L(m, z | T_{\text{gen},1}; \dots; T_{\text{gen},N_{\text{data}}})) \\
 &\stackrel{(2.24)}{=} \ln(f_\gamma(T_{\text{gen},1}; \dots; T_{\text{gen},N_{\text{data}}} | m, z)) \\
 &\stackrel{T_{\text{gen},i} \text{ i.i.d.}}{=} \ln \left(\prod_{i=1}^{N_{\text{data}}} f_\gamma(T_{\text{gen},i} | m, z) \right) \\
 &\stackrel{(2.25)}{=} \ln \left(\prod_{i=1}^{N_{\text{data}}} \left[\frac{z^m}{\Gamma(m)} T_{\text{gen},i}^{m-1} e^{-z T_{\text{gen},i}} \right] \right) \\
 &= \ln \left(\left(\frac{z^m}{\Gamma(m)} \right)^{N_{\text{data}}} \prod_{i=1}^{N_{\text{data}}} \left[T_{\text{gen},i}^{m-1} e^{-z T_{\text{gen},i}} \right] \right) \\
 &= N_{\text{data}} \ln \left(\frac{z^m}{\Gamma(m)} \right) + \sum_{i=1}^{N_{\text{data}}} \ln \left(T_{\text{gen},i}^{m-1} e^{-z T_{\text{gen},i}} \right) \\
 &= N_{\text{data}} m \ln(z) - N_{\text{data}} \ln(\Gamma(m)) \\
 &\quad + (m-1) \sum_{i=1}^{N_{\text{data}}} \ln(T_{\text{gen},i}) - z \sum_{i=1}^{N_{\text{data}}} T_{\text{gen},i}.
 \end{aligned} \tag{2.27}$$

To find a maximum of the likelihood function we first calculate the zero of the partial derivative of \mathcal{L} with respect to z

$$\begin{aligned}
 & \frac{\partial}{\partial z} \mathcal{L}(m, z | T_{\text{gen},1}; \dots; T_{\text{gen},N_{\text{data}}}) = 0 \\
 \stackrel{(2.27)}{\iff} & N_{\text{data}} m \frac{1}{z} - \sum_{i=1}^{N_{\text{data}}} T_{\text{gen},i} = 0 \\
 \iff & \frac{1}{z} = \frac{1}{N_{\text{data}} m} \sum_{i=1}^{N_{\text{data}}} T_{\text{gen},i} \\
 \iff & z = \left(\frac{1}{N_{\text{data}} m} \sum_{i=1}^{N_{\text{data}}} T_{\text{gen},i} \right)^{-1},
 \end{aligned} \tag{2.28}$$

which leads to an explicit estimator for z depending on m and allows to reformulate \mathcal{L} as follows:

$$\begin{aligned}
 & \mathcal{L}(m, z | T_{\text{gen},1}; \dots; T_{\text{gen},N_{\text{data}}}) \\
 &\stackrel{(2.28)}{=} -N_{\text{data}} m \ln \left(\frac{1}{N_{\text{data}} m} \sum_{i=1}^{N_{\text{data}}} T_{\text{gen},i} \right) - N_{\text{data}} \ln(\Gamma(m)) \\
 &\quad + (m-1) \sum_{i=1}^{N_{\text{data}}} \ln(T_{\text{gen},i}) - m N_{\text{data}} \\
 &= N_{\text{data}} \left[m \ln(N_{\text{data}} m) - m \ln \left(\sum_{i=1}^{N_{\text{data}}} T_{\text{gen},i} \right) - \ln(\Gamma(m)) - m \right] \\
 &\quad + (m-1) \sum_{i=1}^{N_{\text{data}}} \ln(T_{\text{gen},i}).
 \end{aligned} \tag{2.29}$$

2 Stochastic modeling predicts paracrine propagation of the IFN response

Utilizing this new formulation (2.29), the partial derivative of \mathcal{L} with respect to m is given by

$$\begin{aligned} & \frac{\partial}{\partial m} \mathcal{L}(m, z | T_{\text{gen},1}; \dots; T_{\text{gen},N_{\text{data}}}) \\ (2.29) \quad & \stackrel{(2.29)}{=} N_{\text{data}} \left[\ln(N_{\text{data}}m) - \ln \left(\sum_{i=1}^{N_{\text{data}}} T_{\text{gen},i} \right) - \frac{\Gamma'(m)}{\Gamma(m)} \right] + m \sum_{i=1}^{N_{\text{data}}} \ln(T_{\text{gen},i}) \quad (2.30) \\ & =: \mathcal{M}(m | T_{\text{gen},1}; \dots; T_{\text{gen},N_{\text{data}}}). \end{aligned}$$

Fulfilling the necessary condition for a maximum of the likelihood function concerning the partial derivative of \mathcal{L} with respect to m supplies an implicit estimate of m :

$$\begin{aligned} & \frac{\partial}{\partial m} \mathcal{L}(m, z | T_{\text{gen},1}; \dots; T_{\text{gen},N_{\text{data}}}) = 0 \\ \stackrel{(2.30)}{\iff} \quad & \mathcal{M}(m | T_{\text{gen},1}; \dots; T_{\text{gen},N_{\text{data}}}) = 0. \quad (2.31) \end{aligned}$$

We determined m independently from z through solving the nonlinear equation (2.31) with the trust-region-dogleg algorithm of Matlab's optimization toolbox (Coleman and Zhang (2003)). Under the usage of the measured data points $T_{\text{gen},i}$, $i = 1, \dots, N_{\text{data}}$ we received $m = 6.4$. Since in the present case m is interpreted as the number of exponentially distributed steps in a stochastic process, m is rounded to the nearest integer. Inserting $m = 6$ in (2.28) yields directly $z = 1.79/\text{h}$. The resulting gamma distribution $\gamma(6, 1.79)$ provides a good approximation of the measured histogram of T_{gen} (cf. Figure 2.13). Therefore we conclude that IFN- β expression after transcription factor activation can be described through 6 consecutive and with rate $k_{\text{IFN}} = 1.79/\text{h}$ exponentially distributed steps. Consequently, each of  first-order processes has a half-life of $\ln(2)/k_{\text{IFN}} = 23\text{min}$. The estimated number of steps and the half-life corresponds well with the mechanistic knowledge about the multi-step formation of the IFN- β enhanceosome (Ford and Thanos (2010)), although transcription and translation might also contribute relevant steps.

In addition, we have observed an average duration of IFN expression in individual cells of $\sim 13\text{h}$. Accordingly, we fixed the rate of termination of IFN- β expression to $l_{\text{IFN}} = 0.08/\text{h}$.

2.4.3 Parameter determination of the IFN response

With the intention to obtain quantitative insight into IFN-induced ISG regulation, we had a closer look on the performed IRF-7 response experiment, in which the IRF-7-mCherry reporter cells were stimulated with increasing units of IFN- β and subjected to flow cytometry at different times after stimulation (cf. Figure 2.7). On the basis of this experiment, we derived a dose-response data set by taking into account the maximal fraction of IRF-7-mCherry $^+$ cells for each applied IFN- β concentration (Figure 2.14). The hyperbolic shape of the derived data set indicates that the dose-response can be characterized by a Hill function

$$R(I) = \frac{I^{h_{\text{IFN}}}}{K_{\text{IFN}}^{h_{\text{IFN}}} + I^{h_{\text{IFN}}}}, \quad (2.32)$$

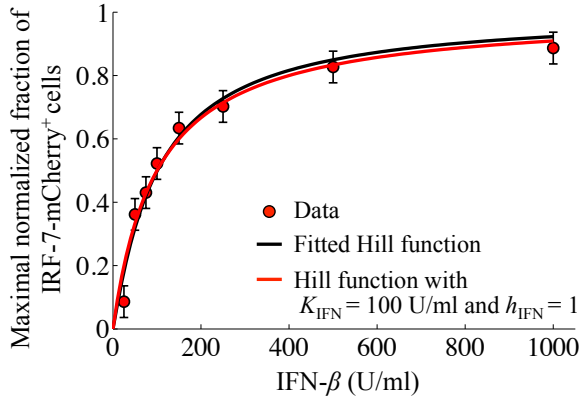


Figure 2.14: Parameter estimation reveals a non-cooperative induction of IRF-7 by extracellular IFN- β . Based on the IRF-7 response measurement (cf. Figure 2.7), we derived a dose-response data set (red dots) by considering the maximal normalized fraction of IRF-7-mCherry⁺ cells (y-axis) for each applied IFN- β concentration (x-axis). The data was fitted with a Hill function (black curve) by applying the trust-region-reflective least-squares algorithm and assuming the indicated 10% measurement error (black error bars). For further simulations we set the fitted parameter values to the whole numbers $K_{\text{IFN}} = 100 \text{ U/ml}$ and $h_{\text{IFN}} = 1$ (red curve). (Experiments by U. Rand, M. Köster and H. Hauser)

whereas K_{IFN} and h_{IFN} denote the half-saturation constant and the Hill coefficient, respectively.

To fit the parameters of the Hill function to the dose-response data set, we utilized the trust-region-reflective least-squares algorithm of Matlab's optimization toolbox (Coleman and Zhang (2003)). The least-squares method is based on the chi-squares statistic

$$\chi^2 = \sum_{i=1}^{N_{\text{data}}} \left(\frac{d_i - y(x_i | p_1, \dots, p_M)}{\sigma_i} \right)^2, \quad (2.33)$$

with the number of observed data points N_{data} , the measured data set (x_i, d_i) , the corresponding measurement error σ_i for $i = 1, \dots, N_{\text{data}}$ and the objective function $y(x_i | p_1, \dots, p_M)$ at x_i with M adjustable parameters p_j for $j = 1, \dots, M$ (Press et al. (2007)).

In the present optimization problem, we considered (2.32) as objective function to describe the derived dose-response data set by assuming a measurement error of 10%. The resulting parameter values $K_{\text{IFN}} = 100.8 \text{ U/ml}$ and $h_{\text{IFN}} = 1.08$ provide an excellent fit to the data (cf. Figure 2.14, black curve). For simulations of the full model we use whole numbers and set $K_{\text{IFN}} = 100 \text{ U/ml}$ as well as $h_{\text{IFN}} = 1$ (cf. Figure 2.14, red curve). The description of the IFN-induced response data by a Hill coefficient with value 1 implies a non-cooperative IRF-7 induction through extracellular IFN- β (Murray (2002)).

In contrast to the dose-response parameters K_{IFN} and h_{IFN} , the rate constants for STAT1/2 activation and ISG induction can be rigorously fitted from the available data. By comparing the simulated kinetic of ISG expression to the experimentally measured one at high viral load (cf. Figure 2.11B, lowest coordinate system), we

2 Stochastic modeling predicts paracrine propagation of the IFN response

detected that $k_{\text{STAT}} = k_{\text{ISG}} = 0.1/\text{h}$ leads to a good match between model and data.

For the determination of the IFN- β secretion rate k_S and the IFN- β degradation rate d_{IFN} , we utilized the measured kinetics of IFN- β -tGFP expressing cells and the amount of released IFN after high-dose infection (cf. Figure 2.11B, second and third coordinate system). Using the preceding parameterization of the IFN- β induction (cf. sections 2.4.1 and 2.4.2) enables the description of the IFN- β -tGFP $^+$ cell fraction over time. Restricted by the kinetic of the IFN- β -producing cells and the already adjusted measurement unit of IFN through fitting $K_{\text{IFN}} = 100 \text{ U/ml}$, we found that $k_S = 0.13 \text{ U}/(\text{h ml cell})$ and $d_{\text{IFN}} = 0.15/\text{h}$ lead to a good agreement between the measured and simulated dynamic of extracellular IFN.

2.5 Stochastic modeling exposes individual IFN producers as sentinels of viral infection

The temporal dynamics of IFN- β -tGFP expressing cells and IFN responding cells after infection with high viral load (cf. Figure 2.11, second and forth coordinate system) suggests that IFN- β secreted by a single cell can induce antiviral ISG production in several cells. To analyze this further, we simulated the model for a range of low-dose infections, where IFN- β -producing cells are sparse  The subsequent comparison of the computed kinetics of IFN responding cells with the measured fraction of ISG-expressing cells showed a good match with the associated data (Figure 2.15A).

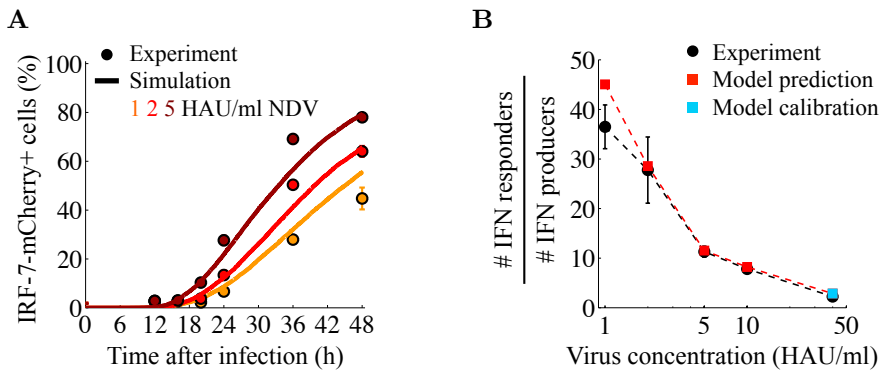


Figure 2.15: Paracrine propagation of the IFN response is predicted by the model and verified experimentally. (A) The model forecasts IFN response for low infection doses. The simulated kinetics of ISG expressing cells (solid curves) can be verified by the measured dynamics of IRF-7-mCherry $^+$ cells (dots) for sparse infections with 1, 2 and 5 HAU/ml NDV. (B) Strong paracrine propagation of the IFN response. Few IFN- β -producing cells at low infection doses induce strong paracrine propagation of the IFN response with up to ~ 40 times as many IRF-7-mCherry expressing cells (IFN responders). The agreement between model (squares) and experimental data (black dots) is remarkable, given that the model was calibrated only for a single condition (40 HAU/ml NDV, marked with blue square) while the red squares represent predictions that were subsequently tested. We considered in each simulation a population consisting of 10^4 cells. (Experiments by U. Rand, M. Köster and H. Hauser)

2.5 Stochastic modeling exposes IFN producers as sentinels of viral infection

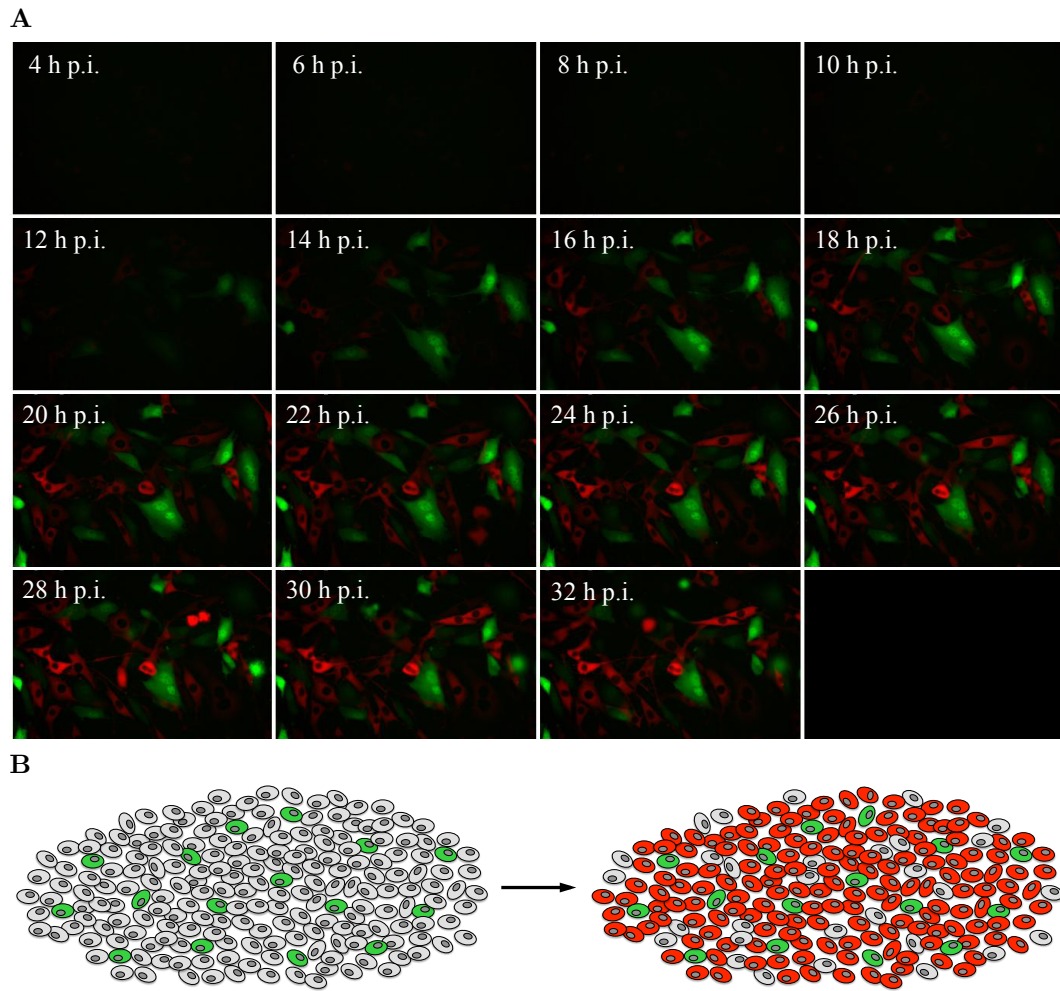


Figure 2.16: Illustrations of the predicted paracrine response communication. (A) Co-culturing of IFN- β -tGFP and IRF-7-mCherry reporter cells illustrates paracrine communication. IFN- β -tGFP reporter cells (green cells) were infected with 40 HAU/ml NDV for 1 h. After this infection period IRF-7-mCherry cells (red cells) were added at same density and cells were subjected to time-lapse microscopy. Merged fluorescent pictures for IFN- β -tGFP and IRF-7-mCherry at indicated time points post-infection are shown. (B) Schematic representation of the assumed protective function of IFN-producing cells. Based on our model simulations, we suggest that few IFN- β expressing cells (green cells) can induce an antiviral gene program in a large number of neighboring cells (red cells) to limit viral spread. (Experiments by U. Rand, M. Köster and H. Hauser)

Importantly, the model predicts strong paracrine amplification of antiviral protection through secreted IFN, with up to 40 times as many ISG-expressing cells than IFN-secreting cells. This model prediction proved remarkably accurate when tested experimentally (Figure 2.15B). Therefore we assume that the paracrine propagation of the IFN response transforms stochastic single-cell behavior into efficient and predictable antiviral protection of the cell population (Rand et al. (2012)). Few IFN-producing cells suffice as sentinels of viral infection to protect a large number of cells surrounding the infection site (Figure 2.16).

3 Spatio-temporal stochastic model of IFN response against viral spread demonstrates homogeneous diffusion

3.1 Dissecting the dynamics of IFN-induced antiviral defense against spreading DENV in living cells

3.1.1 Detection of DENV infection and antiviral IFN response at single-cell level

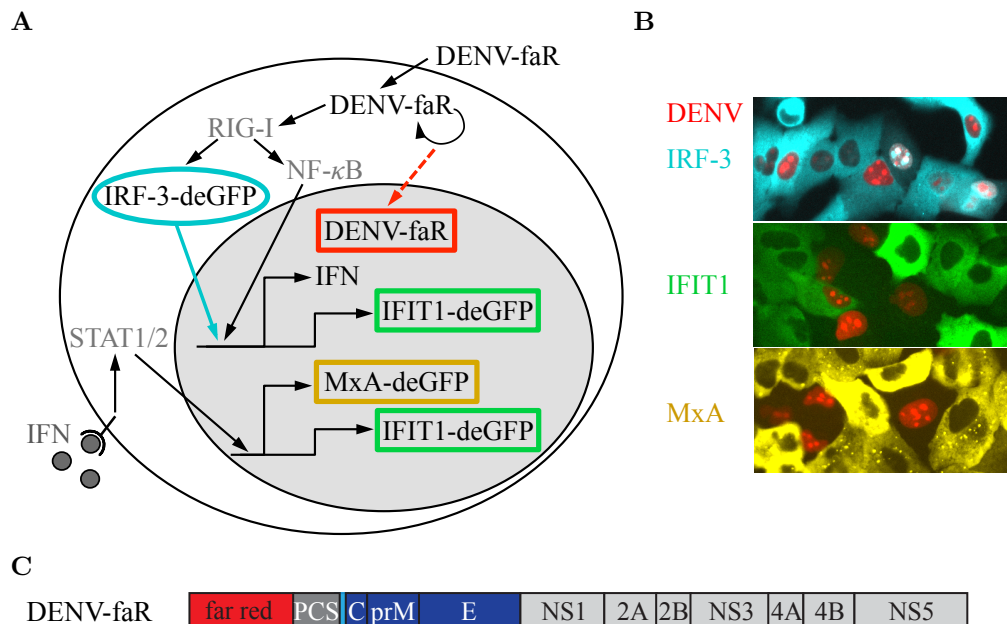


Figure 3.1: (Experiments by B. Schmid and R. Bartenschlager)

3 Spatio-temporal stochastic model of IFN response against viral spread

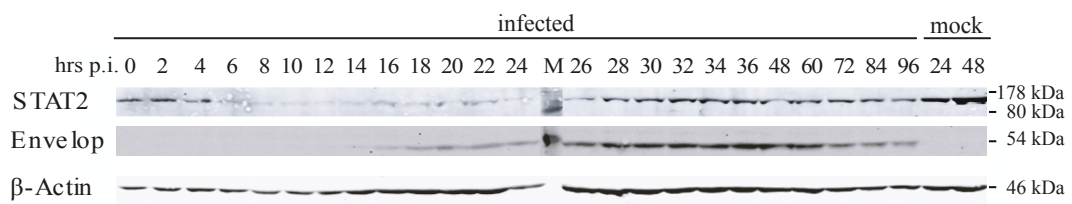


Figure 3.2: (Experiments by B. Schmid and R. Bartenschlager)

3.1.2 The competition between spreading DENV and IFN-induced antiviral protection

3.2 Reaction-diffusion model of viral spread and cell communication through secreted IFN

3.3 Spatio-temporal model simulations show no strong gradients of extracellular virus and IFN

4 Population-based modeling reveals major control of viral fitness by the antiviral effect of IFN on already infected cells

4.1 Quantification of viral spread and the antiviral IFN response

4.1.1 Observation of antiviral protection against DENV-wt infection through IFN stimulation

4.1.2 Examination of viral fitness by comparing DENV-wt with a DENV mutant lacking 2'-O-methylation activity

4.2 Population-based delay-differential equation model of viral spread and IFN-induced antiviral defense

4.3 Parameterization of the DDE model

4.3.1 Estimation of model parameters by using DENV-wt measurements

4.3.2 Detection of DENV mutant specific model parameters by utilizing the knowledge from wt-fitting

4.4 Population-based model predicts strong limitation of viral spread through the impact of IFN on virus production rate

5 Discussion

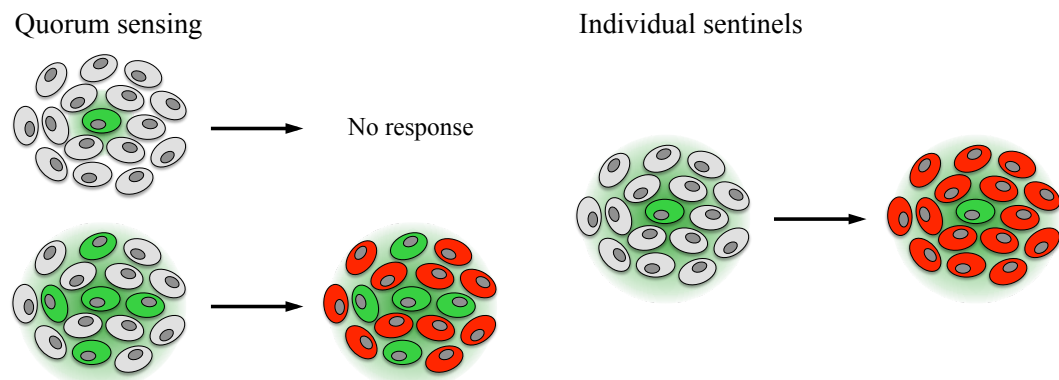


Figure 5.1: IFN expressing cells act as sentinels of viral infection.

Publications and presentations

Bibliography

- Uri Alon. *An introduction to systems biology: design principles of biological circuits.* CRC press, 2006.
- Effie Apostolou and Dimitris Thanos. Virus Infection Induces NF- κ B-Dependent Interchromosomal Associations Mediating Monoallelic IFN- β Gene Expression. *Cell*, 134(1):85–96, 2008.
- Steve Baker and Robert D Cousins. Clarification of the use of chi-square and likelihood functions in fits to histograms. *Nuclear Instruments and Methods in Physics Research*, 221(2):437–442, 1984.
- Harvey Thomas Banks, Anna Broido, Brandi Canter, Kaitlyn Gayvert, Shuhua Hu, Michele Joyner, and Kathryn Link. Simulation Algorithms for Continuous Time Markov Chain Models. 2011.
- Kiva Brennan and Andrew G Bowie. Activation of host pattern recognition receptors by viruses. *Current opinion in microbiology*, 13(4):503–507, 2010.
- Yang Cao and David C Samuels. Discrete stochastic simulation methods for chemically reacting systems. *Methods in enzymology*, 454:115–140, 2009.
- I Capua and DJ Alexander. Human health implications of avian influenza viruses and paramyxoviruses. *European Journal of Clinical Microbiology and Infectious Diseases*, 23(1):1–6, 2004.
- S Chen, JAL Short, DF Young, MJ Killip, M Schneider, S Goodbourn, and RE Randall. Heterocellular induction of interferon by negative-sense RNA viruses. *Virology*, 407(2):247–255, 2010.
- Kay Childs, Nicola Stock, Craig Ross, Jelena Andrejeva, Louise Hilton, Michael Skinner, Richard Randall, and Stephen Goodbourn. mda-5, but not RIG-I, is a common target for paramyxovirus V proteins. *Virology*, 359(1):190–200, 2007.
- T Coleman and Y Zhang. Optimization Toolbox For Use with MATLAB. Natick (MA): The MathWorks. Inc., Sep, 2003.
- Michael B Elowitz, Arnold J Levine, Eric D Siggia, and Peter S Swain. Stochastic gene expression in a single cell. *Science*, 297(5584):1183–1186, 2002.
- Ethan Ford and Dimitris Thanos. The transcriptional code of human IFN- β gene expression. *Biochimica et Biophysica Acta (BBA)-Gene Regulatory Mechanisms*, 1799(3):328–336, 2010.

Bibliography

- Daniel T Gillespie. A general method for numerically simulating the stochastic time evolution of coupled chemical reactions. *Journal of computational physics*, 22(4):403–434, 1976.
- Daniel T Gillespie. Exact stochastic simulation of coupled chemical reactions. *The journal of physical chemistry*, 81(25):2340–2361, 1977.
- Daniel T Gillespie. Stochastic simulation of chemical kinetics. *Annu. Rev. Phys. Chem.*, 58:35–55, 2007.
- Orland R Gonzalez, Christoph Küper, Kirsten Jung, Prospero C Naval, and Eduardo Mendoza. Parameter estimation using Simulated Annealing for S-system models of biochemical networks. *Bioinformatics*, 23(4):480–486, 2007.
- Kenya Honda, Hideyuki Yanai, Hideo Negishi, Masataka Asagiri, Mitsuharu Sato, Tatsuaki Mizutani, Naoya Shimada, Yusuke Ohba, Akinori Takaoka, Nobuaki Yoshida, et al. IRF-7 is the master regulator of type-I interferon-dependent immune responses. *Nature*, 434(7034):772–777, 2005.
- Jianzhong Hu, Stuart C Sealfon, Fernand Hayot, Ciriyam Jayaprakash, Madhu Kumar, Audrey C Pendleton, Arnaud Ganee, Ana Fernandez-Sesma, Thomas M Moran, and James G Wetmur. Chromosome-specific and noisy IFNB1 transcription in individual virus-infected human primary dendritic cells. *Nucleic acids research*, 35(15):5232–5241, 2007.
- Jianzhong Hu, German Nudelman, Yishai Shimoni, Madhu Kumar, Yaomei Ding, Carolina López, Fernand Hayot, James G Wetmur, and Stuart C Sealfon. Role of cell-to-cell variability in activating a positive feedback antiviral response in human dendritic cells. *PloS one*, 6(2):e16614, 2011.
- Mads Kærn, Timothy C Elston, William J Blake, and James J Collins. Stochasticity in gene expression: from theories to phenotypes. *Nature Reviews Genetics*, 6(6):451–464, 2005.
- Hiroki Kato, Shintaro Sato, Mitsutoshi Yoneyama, Masahiro Yamamoto, Satoshi Uematsu, Kosuke Matsui, Tohru Tsujimura, Kiyoshi Takeda, Takashi Fujita, Osamu Takeuchi, et al. Cell type-specific involvement of RIG-I in antiviral response. *Immunity*, 23(1):19–28, 2005.
- David G Kendall. Stochastic processes and population growth. *Journal of the Royal Statistical Society. Series B (Methodological)*, 11(2):230–282, 1949.
- MJ Killip, DF Young, CS Ross, S Chen, S Goodbourn, and RE Randall. Failure to activate the IFN- β promoter by a paramyxovirus lacking an interferon antagonist. *Virology*, 415(1):39–46, 2011.
- K Königsberger. Analysis 1 (6., durchges. Aufl.) (German Edition). Springer, 2004.
- Leo E Kreuz and Allan H Levy. Physical properties of chick interferon. *Journal of bacteriology*, 89(2):462–469, 1965.

Bibliography

- Yutaro Kumagai, Himanshu Kumar, Shohei Koyama, Taro Kawai, Osamu Takeuchi, and Shizuo Akira. Cutting Edge: TLR-Dependent viral recognition along with type I IFN positive feedback signaling masks the requirement of viral replication for IFN-alpha production in plasmacytoid dendritic cells. *J Immunol*, 182(7):3960–3964, Apr 2009.
- Myriam S Kunzi and Paula M Pitha. Interferon targeted genes in host defense. *Autoimmunity*, 36(8):457–461, 2003.
- Doron Levin, Daniel Harari, and Gideon Schreiber. Stochastic receptor expression determines cell fate upon interferon treatment. *Molecular and cellular biology*, 31(16):3252–3266, 2011.
- Björn F Lillemeier, Mario Köster, and Ian M Kerr. STAT1 from the cell membrane to the DNA. *The EMBO journal*, 20(10):2508–2517, 2001.
- Narendra Maheshri and Erin K O’Shea. Living with noisy genes: how cells function reliably with inherent variability in gene expression. *Annu. Rev. Biophys. Biomol. Struct.*, 36:413–434, 2007.
- Tim Maiwald, Annette Schneider, Hauke Busch, Sven Sahle, Norbert Gretz, Thomas S Weiss, Ursula Kummer, and Ursula Klingmüller. Combining theoretical analysis and experimental data generation reveals IRF9 as a crucial factor for accelerating interferon α -induced early antiviral signalling. *FEBS journal*, 277(22):4741–4754, 2010.
- Luca Mariani, Edda G Schulz, Maria H Lexberg, Caroline Helmstetter, Andreas Radbruch, Max Löhning, and Thomas Höfer. Short-term memory in gene induction reveals the regulatory principle behind stochastic IL-4 expression. *Molecular systems biology*, 6(1), 2010.
- I Matheson, DF Walls, and CW Gardiner. Stochastic models of firstorder nonequilibrium phase transitions in chemical reactions. *Journal of Statistical Physics*, 12(1):21–34, 1975.
- Donald A McQuarrie. Stochastic approach to chemical kinetics. *Journal of Applied Probability*, 4(3):413–478, 1967.
- James D. Murray. *Mathematical Biology: I. An Introduction (Interdisciplinary Applied Mathematics) (Pt. 1)*. Springer, 2002.
- In Jae Myung. Tutorial on maximum likelihood estimation. *Journal of mathematical Psychology*, 47(1):90–100, 2003.
- Kazuhide Onoguchi, Koji Onomoto, Shiori Takamatsu, Michihiko Jogi, Azumi Take-mura, Shiho Morimoto, Ilkka Julkunen, Hideo Namiki, Mitsutoshi Yoneyama, and Takashi Fujita. Virus-infection or 5 ppp-RNA activates antiviral signal through redistribution of IPS-1 mediated by MFN1. *PLoS pathogens*, 6(7):e1001012, 2010.
- William H. Press, Saul A. Teukolsky, William T. Vetterling, and Brian P. Flannery. *Numerical Recipes 3rd Edition: The Art of Scientific Computing*. Cambridge University Press, 2007.

Bibliography

- Arjun Raj and Alexander van Oudenaarden. Nature, nurture, or chance: stochastic gene expression and its consequences. *Cell*, 135(2):216–226, 2008.
- Ulfert Rand and Hansjörg Hauser. *Dynamics of Type I Interferon Induction and Action*. 2010.
- Ulfert Rand, Melanie Rinas, Johannes Schwerk, Gesa Nöhren, Melanie Linné, Andrea Kröger, Michael Flossdorf, Kristóf Kály-Kullai, Hansjörg Hauser, Thomas Höfer, and Mario Köster. Multi-layered stochasticity and paracrine signal propagation shape the type-I interferon response. *Mol Syst Biol*, 8:584, 2012.
- Jonathan M Raser and Erin K O’Shea. Noise in gene expression: origins, consequences, and control. *Science*, 309(5743):2010–2013, 2005.
- Andreas Raue, Clemens Kreutz, Thomas Maiwald, Julie Bachmann, Marcel Schilling, Ursula Klingmüller, and Jens Timmer. Structural and practical identifiability analysis of partially observed dynamical models by exploiting the profile likelihood. *Bioinformatics*, 25(15):1923–1929, 2009.
- Jan Rehwinkel, Choon Ping Tan, Delphine Goubaud, Oliver Schulz, Andreas Pichlmair, Katja Bier, Nicole Robb, Frank Vreede, Wendy Barclay, Ervin Fodor, et al. RIG-I detects viral genomic RNA during negative-strand RNA virus infection. *Cell*, 140(3):397–408, 2010.
- R Rott. Molecular basis of infectivity and pathogenicity of myxovirus. *Archives of virology*, 59(4):285–298, 1979.
- Anthony J Sadler and Bryan RG Williams. Interferon-inducible antiviral effectors. *Nature Reviews Immunology*, 8(7):559–568, 2008.
- Johannes Josef Schneider and Scott Kirkpatrick. *Stochastic optimization*. Springer, 2006.
- Berend Snijder and Lucas Pelkmans. Origins of regulated cell-to-cell variability. *Nature Reviews Molecular Cell Biology*, 12(2):119–125, 2011.
- Sabrina L Spencer, Suzanne Gaudet, John G Albeck, John M Burke, and Peter K Sorger. Non-genetic origins of cell-to-cell variability in TRAIL-induced apoptosis. *Nature*, 459(7245):428–432, 2009.
- David G Spiller, Christopher D Wood, David A Rand, and Michael RH White. Measurement of single-cell dynamics. *Nature*, 465(7299):736–745, 2010.
- Peter S Swain, Michael B Elowitz, and Eric D Siggia. Intrinsic and extrinsic contributions to stochasticity in gene expression. *Proceedings of the National Academy of Sciences*, 99(20):12795–12800, 2002.
- Osamu Takeuchi and Shizuo Akira. Innate immunity to virus infection. *Immunological reviews*, 227(1):75–86, 2009.
- Richard Taylor. Interpretation of the correlation coefficient: a basic review. *Journal of diagnostic medical sonography*, 6(1):35–39, 1990.

Bibliography

- Argyrios N Theofilopoulos, Roberto Baccala, Bruce Beutler, and Dwight H Kono. Type I interferons (α/β) in immunity and autoimmunity. *Annu. Rev. Immunol.*, 23:307–335, 2005.
- DJ Venzon and SH Moolgavkar. A method for computing profile-likelihood-based confidence intervals. *Applied Statistics*, pages 87–94, 1988.
- Uwe Vinkemeier. Getting the message across, STAT! Design principles of a molecular signaling circuit. *The Journal of cell biology*, 167(2):197–201, 2004.
- Karl-Heinz Waldmann and Ulrike M Stocker. Stochastische Modelle: Eine anwendungsorientierte Einführung, EMILeAstat, 2004.
- Dirk Werner. *Funktionalanalysis (Springer-Lehrbuch) (German Edition)*. Springer, 2005.
- Rainer Zawatzky, Edward De Maeyer, and Jacqueline De Maeyer-Guignard. Identification of individual interferon-producing cells by *in situ* hybridization. *Proceedings of the National Academy of Sciences*, 82(4):1136–1140, 1985.

Abbreviations and symbols

1_A characteristic function of the set A

\subseteq subset of

\forall universal quantifier; for all

α alpha

β beta

BAC bacterial artificial chromosome

C set of complex numbers

CDF cumulative distribution function

CFP cyan fluorescent protein

CV coefficient of variation

DDE delay-differential equation

ΔT_{gen} time differences between sister cells regarding IFN- β -tGFP expression

ΔT_{sig} time differences between sister cells regarding IRF-7 signaling

DENV dengue virus

DF degree of freedom

dsRNA double-stranded RNA

\in element of

exp(x) = e^x natural exponential function of x

FACS fluorescence-activated cell sorting

FSC forward scatter

γ gamma

$\gamma(m, z)$ gamma distribution with the positive parameters m and z

Γ Gamma

Bibliography

$\Gamma(m)$ gamma function with the positive parameters m

g gram

GFP green fluorescent protein

h hours

H Heaviside step function

HAU haemagglutinating unit

HN hemagglutinin-neuraminidase

HZI Helmholtz Centre for Infection Research

IFN interferon

i.i.d. independent and identically distributed

IRF interferon regulatory factor

ISG interferon stimulated genes

Jak janus activated kinase

κ kappa

λ lambda

l liter

L likelihood function

\mathcal{L} log-likelihood function

mCherry monomeric cherry (red fluorescent protein)

MFI mean fluorescence intensity

μ micro

m milli

min minute

MOI multiplicity of infection

Mx myxovirus resistance protein

N set of natural numbers

NDV newcastle disease virus

NF- κ B nuclear factor kappa B

NIH3T3 mouse embryonic fibroblast cell line

ODE ordinary differential equation

$P(A|B)$ conditional probability of A under the condition B

p.i. post-infection

poly I:C polyinosinic-polycytidylic acid

p65 protein involved in nuclear factor kappa B heterodimer formation

qPCR quantitative polymerase chain reaction

r correlation coefficient

r² coefficient of determination

\mathbb{R} set of real numbers

RIG-I retinoic-acid-inducible gene I

RNA ribonucleinacid

RO readout

RPS9 40S ribosomal protein S9

RSAD2 radical S-adenosyl methionine domain containing 2

SSA stochastic simulation algorithm

STAT signal transducer and activator of transcription

STING stimulator of interferon genes

TagRFP red fluorescent protein tag

T_{div} time of cell division

TF transcription factor

T_{gen} time between nuclear translocation of NF- κ B/IRF-7 and onset of IFN- β expression

T_{gen} simulated time between nuclear translocation of NF- κ B/IRF-7 and onset of IFN- β expression

tGFP turbo green fluorescent protein

T_{sig} signaling delay from viral infection to nuclear translocation of the transcription factors NF- κ B and IRF-7

T_{sig} simulated signaling delay from viral infection to nuclear translocation of the

Bibliography

transcription factors NF- κ B and IRF-7

U unit

USP18 ubiquitin specific peptidase 18

wt wild-type

YFP yellow fluorescent protein

Acknowledgments